2. Band-Structure Determination of Adsorbates

H.-J. Freund and *H. Kuhlenbeck*

We have chosen several examples from the literature to discuss the various aspects of band-structure formation in ordered overlayers. The best suited method to study band-structure formation is Angle-Resolved Ultraviolet Photoelectron Spectroscopy (ARUPS), and in the present chapter exclusively ARUPS data are discussed. The most complete data sets exist for CO adsorbates and we shall outline the various details on the basis of these results. Then, we proceed to discuss hydrocarbon layers of molecules of increasing size, i.e. ethylene and benzene. There are only very few examples of coadsorbates where band structure studies have been undertaken. We shall briefly mention some aspects in the last section of this chapter.

2.1 Historical Introduction

In Langmuir's picture of adsorption [2.1] the adsorbed particles occupy the lattice points of a two-dimensional substrate with equal probability and with hard wall potentials between the adsorbed particles, preventing double or multiple occupancy of any particular site and a well defined adsorption energy typical of the site. As a result saturation would be characterized by $\theta = 1$ and the formation of a true 1×1 absorbate layer. Obviously, the formation of ordered layers with coverages far below $\theta = 1$ are more the exception than the rule and are a direct consequence of the existence of interaction potentials [2.2]. Such an interaction potential is exemplified in Fig. 2.1 for the system CO/Pd(100) reported by *Tracy* and *Palmberg* [2.3] in 1969, compared with a CO–CO interaction potential in the gas phase. Intermolecular interaction potentials may be either attractive or repulsive and may be classified into direct and indirect interactions. Direct interactions involve dipole-dipole (multipole-multipole) and orbital overlap interactions, and are often repulsive. On the other hand, indirect interactions mediated through the metal surface may be either attractive or repulsive depending on distance and surface sites, i.e., the kind of charge modification of the electronic structure of the substrate by the adsorbate [2.4–6]. The interplay of the intermolecular interaction potential and the adsorption energy of the isolated molecule with the clean substrate finally determines the observed structure of an ordered layer. In other words, the
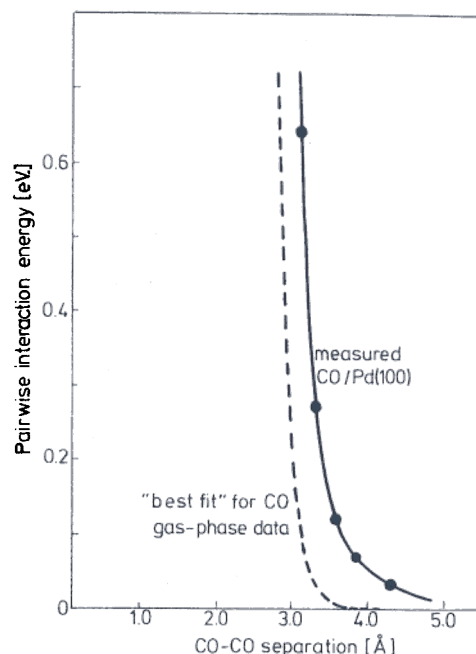
Fig. 2.1. Pairwise interaction energies as a function of intermolecular separation. A CO adsorbate is compared with the gas phase
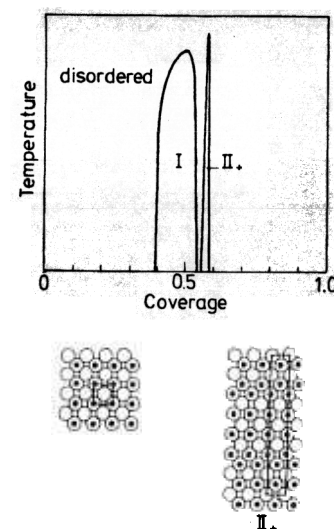

Fig. 2.2. Temperature (T)-Coverage (θ) phase diagram for the system CO/Cu(100). The two areas of ordered structures are indicated and structural models are shown

structure of the ordered layer depends on the heat of adsorption and the coverage. Temperature (T)-coverage (θ) diagrams are usually called *phase diagrams* and have been determined as early as 1972 [2.7]. Figure 2.2 depicts one of the rare examples of a phase diagram of a molecular adsorbate, i.e. CO/Cu(100) [2.8]. CO bound carbon-end down on Cu(100) occupies only on-top sites. In this case two ordered structures, denoted by I and II$_+$ in Fig. 2.2 occur at $\theta = 1/2$ and $\theta = 4/7$, respectively. Phase I is the well known $c(2 \times 2)$ structure while phase II$_+$ consists of stripes of $c(2 \times 2)$ structure of width n = 3 separated by domain walls. The main part of the phase diagram is filled by a disordered phase. It is the well-ordered structure that plays the important role in this chapter as we shall see below.

A way to get insight into intermolecular interactions within adsorbates is to study their electronic structure. Order is particularly important because in the case of two-dimensionally well ordered overlayers the wave vector parallel to the surface ($k_\parallel$) is a good quantum number, and therefore $k_\parallel$ may be observed experimentally. Consequently, it is possible to carry out angle-dependent inelastic electron spectroscopic measurements to determine the $k_\parallel$ dependence of the particular elementary excitation. If we use, for example, electron energy loss spectroscopy (EELS) we get the phonon dispersion relations [2.9] or the plasmon dispersion relations, etc. [2.10]. If we perform angle-resolved photoelectron spectroscopic measurements we get the 'band structure' of the ordered

layers, or better the dispersion relations of the ion states of the system [2.11]. Experimentally, molecular band dispersions were first observed by *Horn* et al. for CO overlayers [2.12]. The experimentally determined band structure can be connected with the intermolecular interaction potential through theoretical modelling. Briefly, in the simplest form of the band-structure formulation, the tight-binding approximation, the bandwidth is determined by the strength of the intermolecular interaction as probed by the particular molecular orbital (ion state) under consideration [2.13]. If it is possible to identify a particular ion state of a molecule in ordered layers of different coverage densities, i.e. varying intermolecular distance, then we are in a position to determine ion state specific intermolecular interaction parameters as a function of intermolecular distance [2.14]. The last point is particularly interesting: Take diatomic molecules with localized orbitals. Assume the molecules interact on one end only with the surface and form an ordered layer. Ionization of an orbital localized on the far end of the molecules away from the surface most likely will lead to a dispersion relation predominantly determined by the direct, or through space interaction [2.15]. If on the other hand we choose to ionize an orbital localized on the near end of the molecules close to the surface, we are going to measure a dispersion relation determined by direct as well as indirect, 'through bond', interaction of the molecules [2.16]. It is therefore possible to use measured ion state specific dispersion relations to study intermolecular interaction mechanisms. It must be understood, however, that experimentally determined band dispersions are excited state properties and intermolecular potentials are usually considered to be ground state properties.

2.2 CO Adsorbates

2.2.1 Symmetry Considerations and CO-Substrate Interactions

CO forms ordered overlayers on most transition metal single-crystal surfaces. Before we turn to the analysis of the denser layers it is important to understand the interaction of an isolated molecule with the clean surface.

With the exception of very few examples, e.g. CO on Cr(110) [2.17], CO on Fe(100) [2.18] and CO on Mo(100) [2.19], where the molecule is tilted, CO is bound vertically towards transition metals if the adsorption energy is characteristic for a chemisorption system [2.20]. Figure 2.3 exhibits two spectra for the chemisorption system CO/Pd(111) for which an adsorption enthalpy of 142 kJ mol^{-1} has been determined. The spectra are taken at different electron-emission angles [2.21]. The top spectrum is taken in the so called 'forbidden' geometry, the spectrum at the bottom in the so-called 'allowed' geometry (see
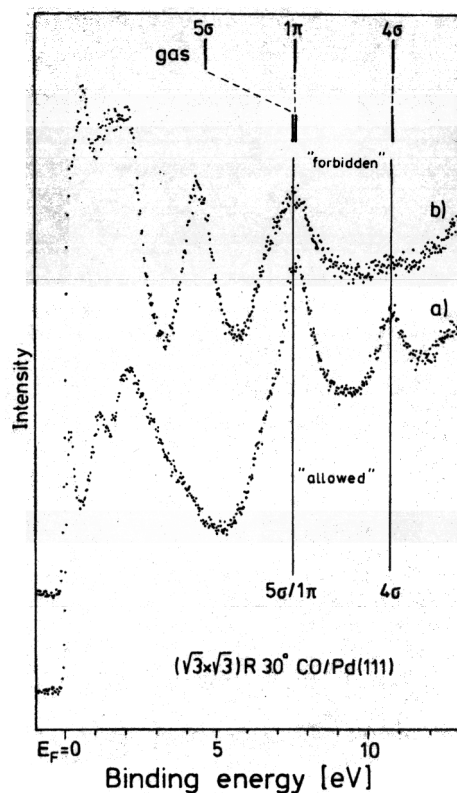

Fig. 2.3. Electron distribution curves in the so called "allowed" and "forbidden" geometries for CO/Pd(111). The positions of the two adsorbate induced features are compared with the positions in the free molecules, where the 4σ-levels have been aligned

below) [2.22]. Characteristic intensity variations are found. First, the bottom spectrum shows two bands, which are typical for a CO chemisorption system and which are shifted by about 2 eV to lower binding energies with respect to the gas phase (see below) [2.22]. The position of the ion states observed in the gas phase as marked in Fig. 2.3 have been aligned artificially to the position to the 4σ ion state in the adsorbate. The intensity variations between the two electron-distribution curves can be used to show that these two CO-induced bands are really caused by the three CO-ion states (5σ, 1π, 4σ) and that the CO molecules are oriented with their axes parallel to the surface normal [2.20, 22]. In order to recall the essentials we shall quickly step through the arguments [2.23, 24] in the following using the results in Fig. 2.3 as an example.

The basis for the discussion is Fermi's Golden Rule:

$$I \propto |\langle \varphi_f|p|\varphi_i\rangle|^2 \qquad (2.1)$$

First, it has to be remembered that φ_f is the final state after electron excitation consisting of the ion state $^{N-1}\Psi_{e,E}$ and the emitted electron $\Phi_e(n)$, and that φ_i represents the neutral ground state of the system. Since p is a one electron operator the matrix element can be rewritten as [2.25]:

$$I \propto |\sum \langle \Phi_e(n)|p_n|\Phi_k(n)\rangle \langle^{N-1}\Psi_{e,E}|a_k\varphi_i\rangle|^2 \qquad (2.2)$$

where a_k and $\Phi_k(n)$ are the annihilation operator and the one-electron wave function of the electron that is being emitted, respectively. These $\Phi_k(n)$ are called initial states in the following.

The first matrix element determines the angular distribution pattern, the second matrix element defines the absolute value and contains the internal degrees of freedom of the system, e.g., the line widths [2.25]. The sum takes all possible ion states $^{N-1}\Psi_{e,E}$ into account and explains the existence of satellite structure [2.25]. Since we are interested in ARUPS, much of the discussion will concentrate on the first matrix element. Second, in order to evaluate whether this matrix element is non zero, and thus leads us to expect a finite photoelectron current in a specific direction in space, symmetry arguments can be used. In principle the space group of the adsorbate under consideration has to be chosen, and then we have to classify the wave functions according to their irreducible representations. Often, it is sufficient to consider one specific symmetry operation belonging to the point group, instead of all possible symmetry operations, in order to predict the angular variations of electron emission. In the present case we refer to one of the mirror planes of the Pd(111) surface. If we classify the wave functions of the electron Φ_e and Φ_k, as well as the momentum operator p to be 'even' or 'odd' with respect to this mirror plane, we are in the position to differentiate between 'even' and 'odd' initial states by choosing certain light polarizations and detecting the angular-distribution pattern as long as spin-orbit interaction is not important [2.26]. For the above given situation the light incidence angle is 90° with respect to the surface plane and the light polarization direction is within the mirror plane. This corresponds to even symmetry of the momentum operator with respect to the mirror plane. Therefore, initial states

with even symmetry will emit in the direction of the mirror plane because the final states have to be even in order for the matrix element not to vanish. In principle, one would expect a finite emission probability along the whole mirror plane. In the present case, however, one has to take into account the cylindrical symmetry of a CO molecule, bonded linearly towards the metal surface. Even initial states of a cylindrical molecule cannot emit in the direction given by the plane perpendicular to the mirror plane which contains the light polarization vector. This latter property can easily be understood if we remember that any plane in a cylindrical system containing the cylindrical axis is a symmetry plane. Combining this property with the fact that the momentum operator is odd with respect to this second plane (perpendicular to the light incidence) means that there cannot be any emission of even states in this direction. Therefore, in order to fulfill both conditions simultaneously, we do not expect an intense CO-4σ emission along the surface normal for light polarized in the surface plane. 4σ emission along the surface normal can only be achieved by using a light polarization perpendicular to the surface plane because in this case the momentum operator is even with respect to any plane perpendicular to the surface plane. If we combine the considerations so far, we verify the above angular distribution pattern.

As a consequence of the outlined behaviour of even initial states, we expect a complementary behaviour of odd initial states. This is exactly what is observed experimentally and is shown as a set of electron distribution curves - which is the usual way to look at ARUP-spectra-in Fig. 2.3. In this figure the complementary behaviour of σ and π emissions, which was first observed by *Lapeyre* and co-workers [2.27, 28] and then by *Plummer* and coworkers [2.22], is obvious: If we record a spectrum perpendicular (so-called *forbidden geometry*) to the incidence plane we do not observe emission in the region of the 4σ level but only in the region of the $5\sigma/1\pi$ levels. Note, that the 1π-ion states of CO has two degenerate components, one of which is always even with respect to a certain mirror plane. Thus, we expect to see the one odd component of the 1π-ion state. A spectrum recorded with the analyzer placed within the incidence plane, the so called *allowed geometry*, shows all states with even symmetry. From Fig. 2.3 it is clear that the feature at 8 e V below the Fermi energy contains two states, i.e. the 1π- and the 5σ-ion states. Their energies are, in contrast to the gas phase, nearly (within a few tenths of 1 e V) degenerate in the adsorbate [2.22]. This is due to the donation of the 5σ carbon lone pair into empty metal levels, thus stabilizing the CO 5σ level with respect to the 1π level which is not as intimately involved in the molecule-metal interaction for linear metal-molecule bonding [2.29, 30], a situation similar to that proposed in the introduction.

The adsorbate induced features exhibit, in addition to the described angular dependence [2.31], characteristic photon-energy dependencies, which, when recorded in an angle-dependent fashion, can be used to get further information about adsorbate site geometry [2.22]. Figure 2.4 shows a plot of the intensity of the 4σ-ion state as a function of photon energy. The data have been recorded for the system CO/Co(0001) [2.15] for three different electron emission angles. The
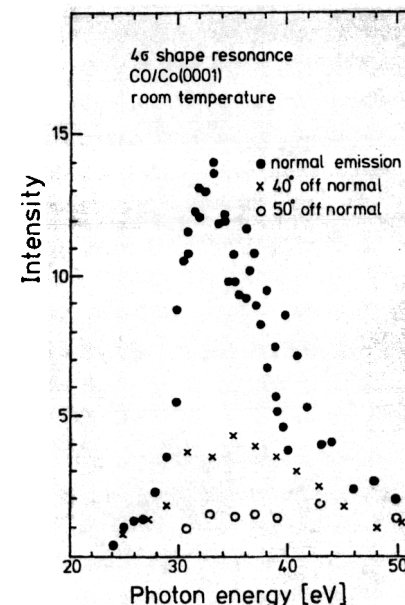

Fig. 2.4. 4σ shape resonances at three electron emission angles for the system CO/Co(0001)

observed resonance feature is caused by the so called *shape resonance*, which is well known from CO gas phase studies [2.32, 33]. It can be traced back to a molecular final state of σ symmetry in the ionization continuum, quasi-bound by a centrifugal barrier in the molecular potentials. Its symmetry confines the electron emission direction to the molecular axis, and directs the 4σ emission out of the oxygen end of the molecule. This means that for the case of a molecule oriented along the surface normal, carbon-end bound to the surface, the resonance should peak along the surface normal. Experimentally, we find in Fig. 2.4 the expected behaviour, i.e., a pronounced attenuation of the resonance intensity for off-normal emission, which corroborates the assumed adsorbate orientation. This is true basically for all CO chemisorbates on transition-metal surfaces.

2.2.2 Ordered Overlayers

a) Chemisorbed Layers

The next step is to consider an ordered overlayer. As an introduction to the quasi two-dimensional band structure of molecular overlayers we discuss the band dispersions and the symmetry properties of a hexagonal overlayer [15] of CO molecules on a (111) surface. If the intermolecular interaction potential is

large enough to demand consideration of the two-dimensional crystal periodicity, the overlap of adsorbate wave functions is sufficient to produce two-dimensional Bloch states Ψ_k and to make a band description of the electronic structure more appropriate [2.12]. Then the one-electron wave function at a lattice site R_1 is related to the wave function at site R_2 by

$$\Psi_k(R_1) = \Psi_k(R_2)\exp[ik_\parallel \cdot (R_1 - R_2)] \qquad (2.3)$$

where $\exp[ik_\parallel \cdot (R_1 - R_2)]$ gives the phase difference between the two sites for a state specified by the two-dimensional wave vector $k_\parallel$. Before we consider the changes in the band structure introduced by the substrate we will briefly discuss the qualitative behaviour of the band dispersion of a hypothetical support free molecular layer [2.34], as shown in Fig. 2.5. We can illustrate the qualitative features of the dispersion by plotting schematically the real parts of a tight-binding wave function in real space for values of $k_\parallel$ corresponding to high symmetry points in reciprocal space. Figure 2.6 depicts the real- and reciprocal-space unit cells for the hexagonal structure. The real and reciprocal lattices have two different types of mirror planes, one along the $\bar{\Gamma}$-$\bar{M}$-$\bar{\Gamma}$ line (in reciprocal
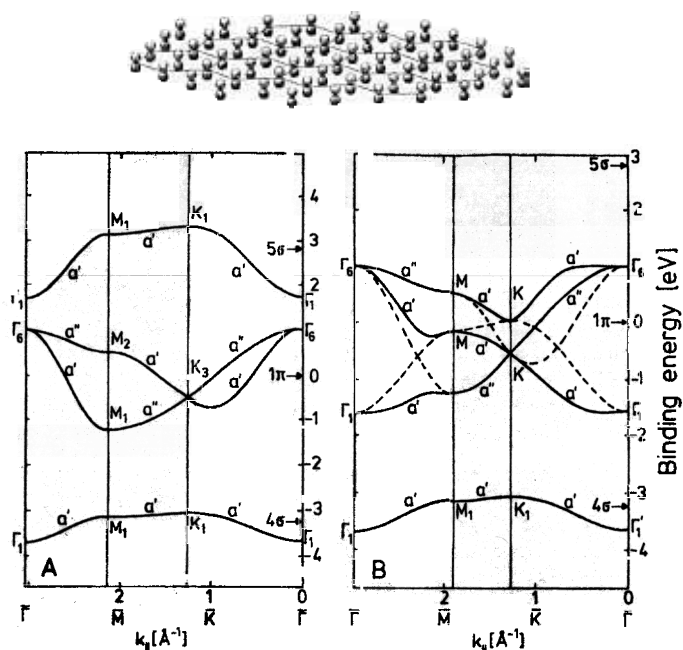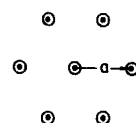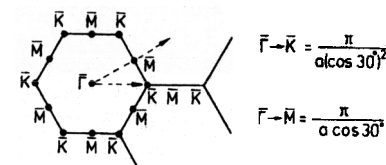

Fig. 2.5. Calculated band structure of a free unsupported hexagonal CO layer. In the left panel the bands are centered at the positions of the free molecule. In the right panel the 5σ-level has been shifted to center the band of the 1π-band center in order to demonstrate possible hybridization effects
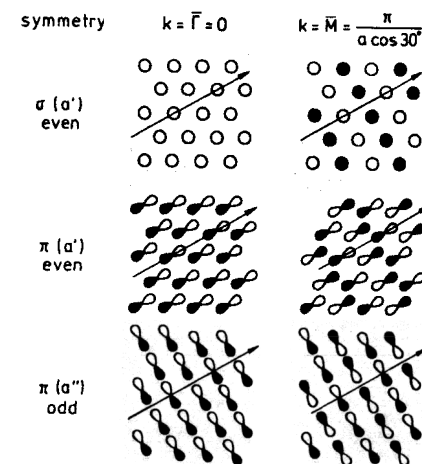

A

B

Fig. 2.6A, B. Schematic two-dimensional wave functions of a hexagonal CO layer along the $\bar{\Gamma} \rightarrow \bar{M}$ direction A real and reciprocal space representation of the hexagonal layer B wave functions

space), and the other one along the line $\bar{\Gamma}$-$\bar{K}$-$\bar{M}$-$\bar{K}$. The wave functions along these lines will be even (a') or odd (a''). Figure 2.6 illustrates the phases of a σ-state and the two π-states at $\bar{\Gamma}$ and $\bar{M}$. At $\bar{\Gamma}(k_\parallel = 0)$ all the wave functions at the different lattice sites are in phase. This results in a strongly bonding configuration for the σ-state (top row), but an anti-bonding configuration for both π-states because the individual π-functions change sign about the molecular axis. The π-functions have been chosen so that one is even and one is odd with respect to the $\bar{\Gamma}$-$\bar{M}$ mirror plane. Because at $\bar{\Gamma}$ the wave functions transform according to C_{6v}, the two π-components are degenerate. Therefore, at $\bar{\Gamma}$ we have a strong bonding σ-band and a degenerate antibonding π-band. Along the mirror plane $\bar{\Gamma}$-$\bar{M}$ $k_\parallel$ increases from 0 at $\bar{\Gamma}$ to $\pi/a\cos 30°$ at the zone boundary $\bar{M}$. The second column shows the wave functions at $\bar{M}$ where the arrow

indicates the direction of $k_\parallel$. All rows of atoms parallel to $k_\parallel$ have the same phase but the phases of neighbouring rows differ by π. The result for the σ-states is that each atom is surrounded by four atoms of opposite phase (antibonding) and two bonding atoms. The σ-bands therefore disperse upward from $\bar{\Gamma}$ to $\bar{M}$. In contrast, the even π-state is strongly bonding since each lobe of the molecular π orbitals sees only bonding nearest neighbours. The even π-band disperses downward from $\bar{\Gamma}$ or $\bar{M}$ with the largest difference in the π-band energy. The odd π-state at $\bar{M}$ is just slightly more bonding than the π-state at $\bar{\Gamma}$ since the overlap of the lobes in a line perpendicular to $k_\parallel$ is antibonding but the overlap between the lines of atoms is bonding. This means that at $\bar{M}$ the two π derived bands are no longer degenerate as a consequence of the lower symmetry of the $\bar{M}$ point. Thus, we have explained the qualitative features of the dispersions in the $\bar{\Gamma}$ of $\bar{M}$ direction shown in Fig. 2.5. Analogously, the dispersions in the other directions of high symmetry in the surface Brillouin zone can be explained, and we refer to the literature for a more detailed discussion [2.15].

Such dispersions can be determined via ARUPS, as shown in Fig. 2.7, where spectra of a $(2\sqrt{3} \times 2\sqrt{3})R30°$ CO/Co(0001) overlayer for different values of the wave vector $k_\parallel$ are plotted [2.15]. The wave vector is varied by varying the photon energy and the emission angle θ within the direction of the considered surface azimuth as noted in the figure. The connection between $k_\parallel$ and the varied quantities is given by

$$k_\parallel = (2m_e \hbar^{-2} E_{kin})^{1/2} \sin\theta \qquad (2.4)$$

where $k_\parallel$ is the wave vector parallel to the surface, which is the conserved quantity, E_{kin} is the kinetic energy of the escaping electron with respect to the vacuum level. Figure 2.8 displays a comparison of calculated dispersions for the 4σ derived band with measured 4σ dispersions of CO/Co(0001) adsorbates in $\bar{\Gamma}$-$\bar{M}$ direction of the hexagonal $(\sqrt{3} \times \sqrt{3})R30°$ and $(2\sqrt{3} \times 2\sqrt{3})R30°$ layers (partially based on Fig. 2.7). We have artificially set the lengths of the two Brillouin zones equal for a more convenient comparison. Due to the smaller CO–CO distance in the $(2\sqrt{3} \times 2\sqrt{3})R30°$ layer, the overlap of the 4σ CO wave functions increases, and concomitantly, the *bandwidth* increases. Figure 2.8 illustrates that the increase in bandwidth can be quantitatively reproduced by simple tight-binding calculations (full lines) in the case of 4σ derived bands. In the present case the comparison can be made directly because the number of nearest neighbours is the same in both systems. If, on the other hand, we want to compare dispersions in hexagonal and quadratic systems, the observed bandwidths have to be corrected for the different numbers of nearest neighbours. Such a correction is straightforward on the basis of simple tight-binding considerations. The results of such a comparison for several different adsorbate systems is exhibited in Fig. 2.9 [2.12, 15, 16, 34–42]. The data points follow an exponential dependence on the nearest-neighbour distance with a characteristic decay length of 1.23 Å if we disregard the CO–K co-adsorbate for the moment. This strongly supports the conclusions that the 4σ-dispersion is caused by direct CO–CO overlap. Intuitively, this is reasonable, because the 4σ CO level is not

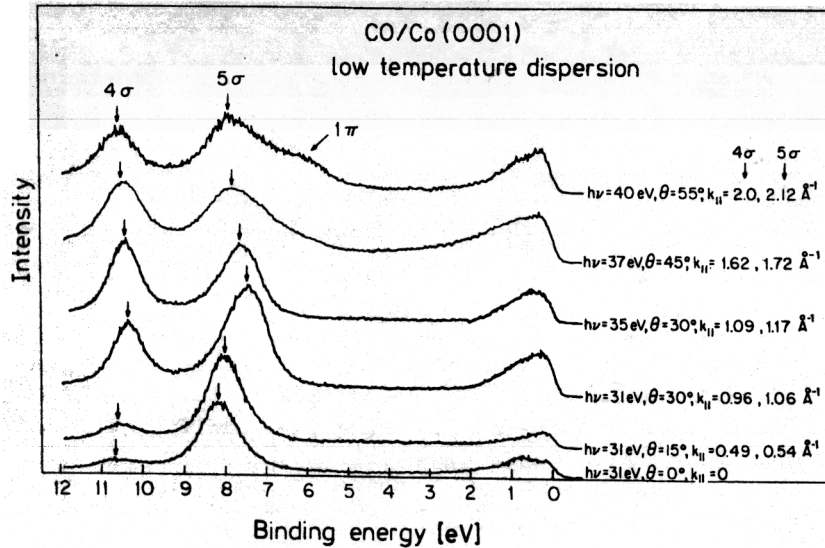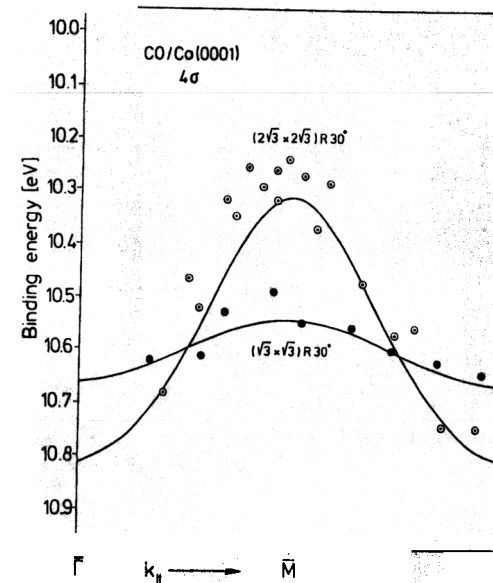**Fig. 2.7.** Electron distribution curves for the system $(2\sqrt{3} \times 2\sqrt{3})R30°$ CO/Co(0001) taken at different excitation and electron emission conditions

Fig. 2.8. Comparison of experimental and theoretical dispersions for two CO overlayers on Co(0001) of varying CO density
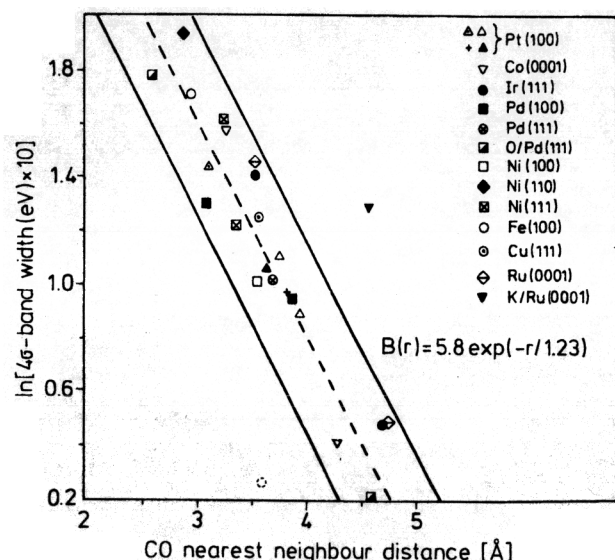
Fig. 2.9. Observed 4σ-bandwidth as a function of intermolecular separation. Six nearest neighbour are used as reference

strongly involved in the metal substrate bonding. At the same time we expect a completely different behaviour for the 5σ-level, because in this case the interaction with the substrate should have a marked influence on the measured dispersion. There is no such simple exponential dependence of the observed bandwidth on the CO–CO distances as for the 4σ-level [2.16]. A similar plot for the 5σ-level exhibits no particular functional dependence, which may be an expression of the participation of indirect through substrate interactions in the intermolecular interaction. Care has to be exercised not to jump to this conclusion prematurely, because, due to the stabilization of the 5σ-level in the region of the 1π-level we expect strong $5\sigma/1\pi$ hybridization effects which have to be taken into account in the prediction of band dispersions [2.15]. For the case of the hexagonal CO layer this situation is depicted in Fig. 2.5 on the right-hand side.

In spite of the vast knowledge on CO adsorbates on solid surface there are only very few examples where detailed and rather complete experimental information on the band structure has been collected. One example is the $CO(2 \times 1)p2mg/Ni(110)$ system [2.37, 2.46–48] which we want to consider in greater detail in the following. Exposure of a clean Ni(110) surface to CO at $T \sim 120$ K leads to the formation of a dense CO overlayers with coverage $\theta = 1.0$ which gives rise to a (2×1) LEED (Low Energy Electron Diffraction) pattern [2.49]. This LEED pattern is characterized by spot extinctions along the

[$1\bar{1}0$] direction indicating that the layer has $p1g1$ or $p2mg$ symmetry. X-ray Photoelectron Diffraction (XPD) [2.50] and Electron Stimulated Desorption Ion Angular Distribution (ESDIAD) [2.51] as well as ARUPS studies showed that the structure actually exhibits $p2mg$ symmetry; a structure model is depicted in Fig. 2.10. The CO molecules are canonically bound carbon-end down and tilted along the [001] azimuth in order to avoid the close intermolecular contact along [$1\bar{1}0$] with a separation below 3 Å which would occur if the molecules were perpendicularly oriented [2.49–54].

Figure 2.11 illustrates the full band structure of the system. The occupied part was determined by measuring the binding energies of the CO induced features as a function of the electron-emission angle along two azimuths with respect to the Ni(110) substrate, i.e. the [$1\bar{1}0$] and the [001] directions. Together with the experimental data [2.37, 2.46–48] we have plotted the result of a band-structure calculation where the position of the lowest occupied $4\sigma^+$-valence orbital (see below) has been shifted to agree with experiments and the tilt angle has been used as a parameter. The best fit resulted for a tilt angle of $17°$ with respect to the surface normal. On the right-hand side of the collected dispersion data we show a set of photoelectron spectra at the Γ point (normal emission). Clearly, the number of outer valence features which are found at binding
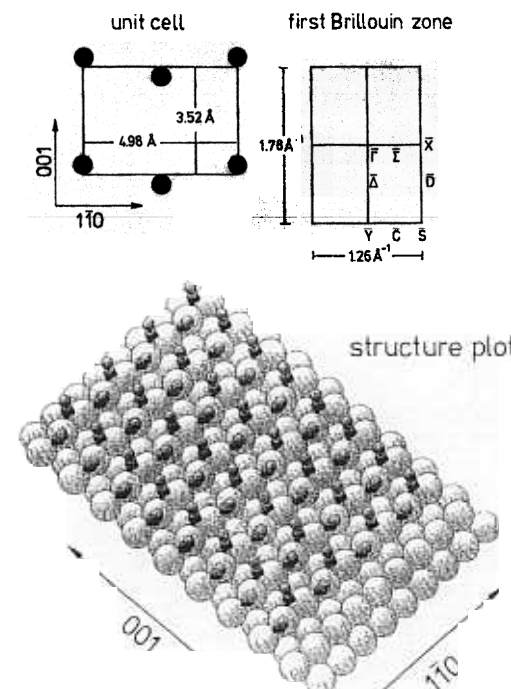

Fig. 2.10. Schematic representation of the $CO(2 \times 1)p2mg/Ni(110)$ structure, the unit cell and the surface Brillouin zone
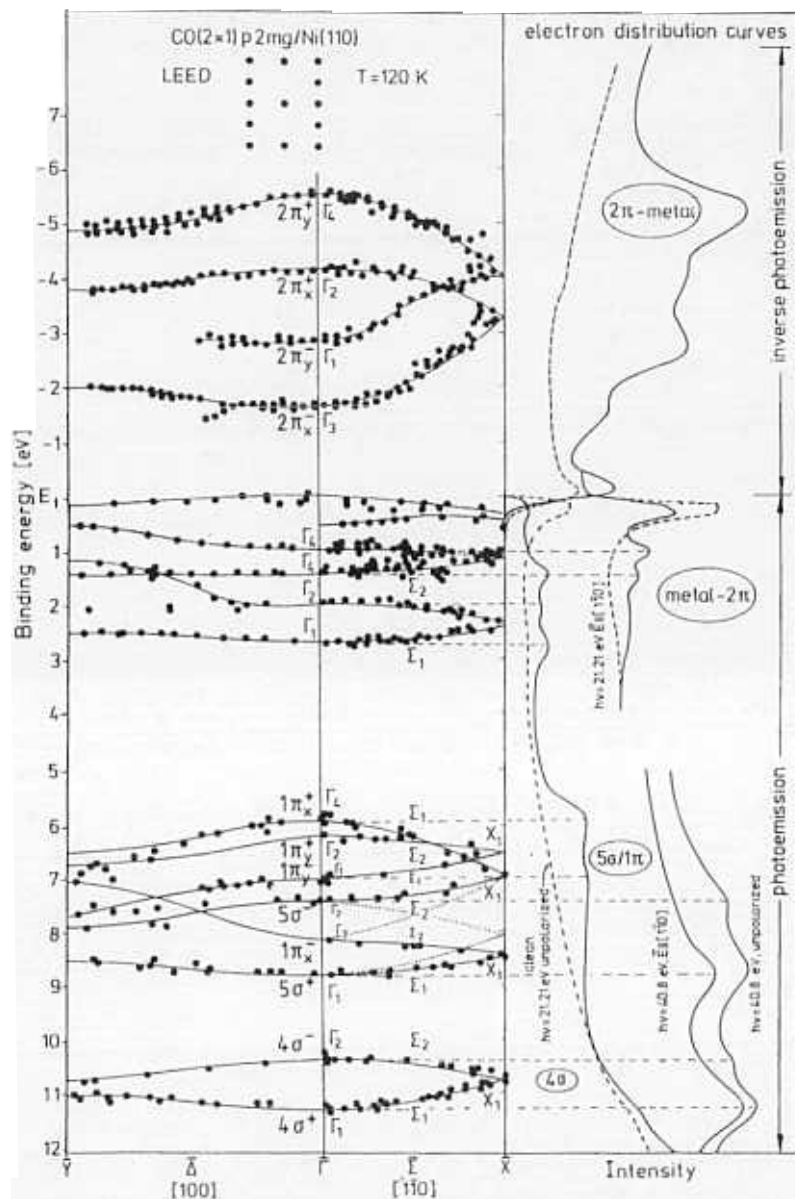
Fig. 2.11. Occupied and unoccupied band structure for $CO\,p2mg/Ni(110)$. In the right panel some typical electron distribution curves are shown

energies above 6 eV is larger than four, which would be the maximum number of features for a single molecule within the unit cell (5σ, 4σ and two 1π components). This indicates that the unit cell contains more than one molecule [2.37]. The region of the energetically well separated 4σ-emissions reveals a splitting into two features consistent with two molecules in the unit cell.

For a description of the band structure the wave functions of a single molecule are therefore not appropriate. However, linear combinations

$$\chi_1 = c_1|CO^1\rangle + c_2|CO^2\rangle \qquad \text{symmetric}$$

and

$$\chi_2 = c_1|CO^1\rangle - c_2|CO^2\rangle \qquad \text{asymmetric} \qquad (2.5)$$

of molecular CO wave functions located at the positions of the two molecules within the unit cell allow one to construct two-dimensional adlayer wave functions that transform according to $p2mg$ symmetry and which give rise to bands (E vs. $k_\parallel$) easy to label by their irreducible representations at the points of high symmetry. Figure 2.12 schematically displays two-dimensional adlayer wave functions at $\bar{\Gamma}$, $\bar{X}$, and $\bar{Y}$ based on σ molecular wave functions (Fig. 2.12a). The unit cell is indicated, χ_1 and χ_2 are plotted. Consider Fig. 2.12a to represent the 4σ-orbitals of CO. Unlike the case of one molecule per unit cell leading to a single band per non-degenerate Molecular Orbital (MO) in the Brillouin zone, we have two bands in the present case, namely, one associated with the symmetric, the other one with the asymmetric combination of molecular orbitals. In the band structure the bands are labelled $+$ and $-$, respectively. At $\bar{\Gamma}$ the splitting of the two 4σ derived bands is about 0.85 eV, caused by the strong lateral interaction. In the symmetric combination all MOs have the same phase, i.e, the two-dimensional wave function is strongly bonding which leads to a stabilization on a binding energy scale compared to a laterally non-interacting adsorbate. The asymmetric combination at $\bar{\Gamma}$ is antibonding with respect to the direction of the glide plane [$1\bar{1}0$], but bonding with respect to the [001] direction. The interaction is stronger along the close packed [$1\bar{1}0$] direction leading to a net destabilization on a binding energy scale. If we follow the bands in $k_\parallel$-space along $\bar{\Gamma} - \bar{X}$ (the $\bar{\Sigma}$ direction), the $+$ band increases, while the $-$ band decreases in energy until they are degenerate at $\bar{X}$. Figure 2.12a allows us to visualize the situation: At $\bar{X}$ the phase between adjacent unit cells changes by 180° along [$1\bar{1}0$]. Consequently, for the symmetric combination this yields a two-dimensional wave function with phase changes only between rows in [001] direction. For the asymmetric combination a similar wave function results which is evident from Fig. 2.12a. In fact, these wave functions are degenerate. As was shown by *Hund* [2.55] the bands have to be degenerate on the entire line $\bar{X} - \bar{S}$, which is perpendicular to the glide plane (Fig. 2.10). Clearly, the wave function plots indicate that the energy position of the bands at $\bar{X}$ has to be intermediate between the energies at $\bar{\Gamma}$ since there is increasing antibonding character for the symmetric combination while there is loss of antibonding character for the asymmetric combination. At $\bar{Y}$ the wave functions and thus the
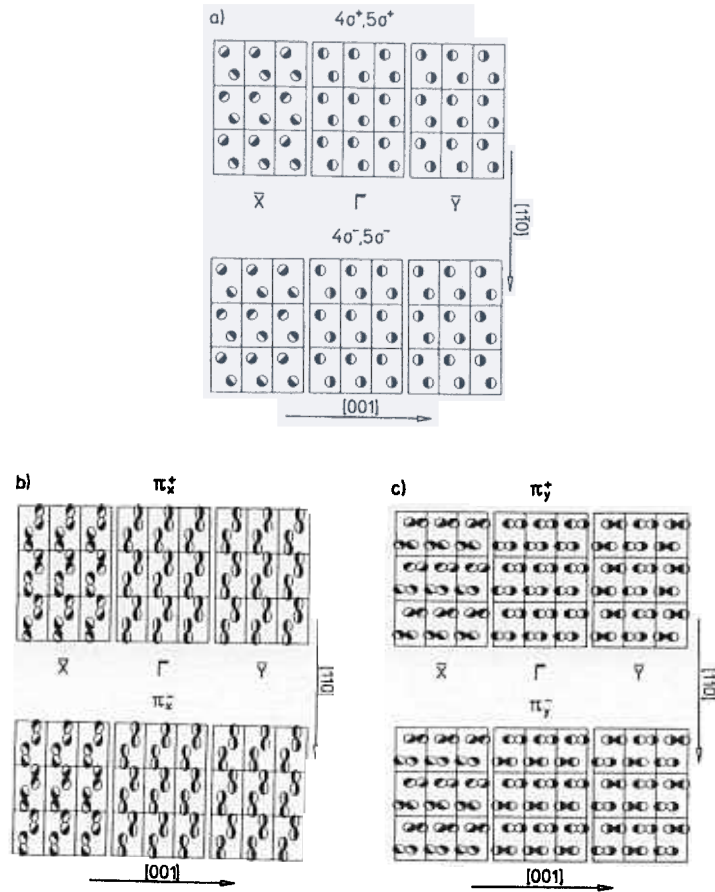
Fig. 2.12a-c. Schematic representation of the σ (a) and π (b, c) derived wave functions of the CO overlayer for different k-points. Each orbital lobe is half hatched. The direction of the line separating open and hatched part of the lobe marks the phase of the respective molecular wave function. In the zero phase situation the direction of the separating line points along the [1$\bar{1}$0] direction and the left part of the lobe is hatched

bands are non-degenerate energetically, since the spatial separation between sites of equal phase is larger for the $-$ than for the $+$ band. The splitting at $\bar{Y}$ is 0.3 eV, which should be compared with 0.85 eV at $\bar{\Gamma}$. In order to specify the character of the wave functions within the band-structure plot the irreducible representations of the wave functions are indicated.

Next, we consider the region of the band structure of occupied levels at lower binding energies, namely, the region of the 5σ and 1π molecular orbitals. Due to the low symmetry of the overlayer 5σ and 1π derived adlayer bands are

allowed to hybridize. The solid lines in this region (Fig. 2.11) refer to the bands after hybridization has been taken into account, while the dotted lines refer to the non-hybridized bands. We start the discussion by first considering the band dispersion neglecting hybridization. Clearly, the dispersion of the nonhybridized 5σ-bands should be similar to the 4σ-dispersion. In fact, this is our result. The splittings calculated for various symmetry points, however, differ considerably. This is expected since the spatial extent of the 5σ molecular orbitals is different from the 4σ molecular orbitals. This aspect has been discussed in detail by *Greuter* et al. [2.15]. Compared with the 4σ-bands the 5σ-bands show a splitting of 1.35 eV at $\bar{\Gamma}$ and 0.63 eV at $\bar{Y}$ since the 5σ molecular orbitals are more diffuse than the 4σ molecular orbitals.

The dispersions associated with the nonhybridized 1π molecular orbitals are due to their twofold degeneracy on the molecular level, slightly more complicated than the σ-band dispersions. Since the global symmetry of the adlayer is only twofold, the two 1π-components cannot be degenerate and, due to the formation of symmetric and asymmetric combinations, give rise to four bands at $\bar{\Gamma}$. In order to label the bands, we have chosen x to denote the component in [1$\bar{1}$0], y to denote the component in [001] direction. The wave functions belonging to the x components are exhibited in Fig. 2.12b. Again, symmetric and asymmetric phase relations are identical to those for the σ-bands shown in Fig. 2.12a. Unlike the σ-bands, however, the antibonding combination is symmetric (+) and the bonding combination is asymmetric ($-$) in the 1π-case. As outlined above, the + or $-$ sign refers to phase factors within the unit cell, while bonding and antibonding refers to the interaction of the wave functions within the unit cell: An in-phase combination of two π functions is antibonding and thus energetically destabilized, the out-of-phase combination of two π functions is bonding and thus energetically stabilized. In other word, π bands associated with phase factors + and $-$ are energetically reversed with respect to the σ-bands. The splitting between + and $-$ bands differs for the x and y components, in agreement with expectations since the lateral interactions along [1$\bar{1}$0] are much stronger than along [001]. The magnitudes of the splitting are 2.1 eV and 0.78 eV at $\bar{\Gamma}$, respectively. At $\bar{\Gamma}$, $1\pi_x^+$, $1\pi_x^-$, $1\pi_y^+$ and $1\pi_y^-$ all belong to different irreducible representations. At $\bar{X}$ the bands are pairwise degenerated for the same reason we used for the σ-bands. The bonding character of the wave functions at $\bar{X}$ is clearly higher for the x-component than for the y-component as is evident from Fig. 2.12b and 2.12c. Along the $\bar{\Sigma}$ line there are only two irreducible representations. The bands are labelled according to *Litvin*'s compatibility relations [2.56]. The $1\pi_x^-$-band has the same symmetry as the $1\pi_x^{-1}$ band along $\bar{\Sigma}$, leading to a very small gap around the crossing point. The gap is very small since the interaction is 'weak' for topological reasons. Perpendicular to the $\bar{\Sigma}$ direction, namely in the $\bar{\Delta}$ direction, the π-bands, like the σ-bands, are not degenerate at the zone boundary. Along the $\bar{\Sigma}$ direction the two $1\pi_y$-bands cross and, having the same symmetry, are allowed to hybridize. Figure 2.12c shows on the right hand side that the $1\pi_y^-$-band is, in addition to its bonding character in [001], antibonding along [1$\bar{1}$0]. The $1\pi_y^+$-band is

bonding in both directions. σ/π-hybridization can only occur if the bands for π and σ parentage transform according to the same irreducible representations. Along $\bar{\Gamma}$-$\bar{X}$, i.e. in the $\bar{\Sigma}$-direction, the $1\pi_x^-$-band hybridizes with the $5\sigma^-$-band shifting the energetic position of the point of degeneracy. Note that the degeneracy at $\bar{X}$ is not lifted by σ/π-hybridization. However, it is evident that the hybridized band structure is considerably different from the nonhybridized one. At $\bar{\Gamma}$, for instance, the σ/π-hybridization leads to reversal of the $1\pi_y^-$ and $1\pi_y^+$ binding energies.

So far we have discussed the development of the band structure without explicit reference to the experimental observations. The basis for an experimental analysis is Table 2.1 where the dipole selection rules for the $p2mg$ system at $\bar{\Gamma}$ are summarized. At $\bar{\Gamma}$ the symmetry is C_{2v} and the symmetry selection rules shown in Table 2.1 may be applied. Because the final state of the electron must be totally symmetric (Γ_1) there is evidence for a Γ_2- and a Γ_1-state in the range of the 4σ-ionization if we compare the spectra recorded with polarized (electric field vector E parallel to the $[1\bar{1}0]$ direction) and unpolarized light in Fig. 2.11. The symmetry restrictions for the $4\sigma^-$- and $4\sigma^+$-bands hold in the same way for the $5\sigma^-$- and $5\sigma^+$-bands. The comparison of the same two spectra supports this conclusion. If the photon energy is smaller, i.e. around 20 eV, the cross section of the π derived components becomes more prominent. The π derived Γ_4-band at lowest binding energy can be well used to demonstrate that the symmetry of the ordered overlayers is $p2mg$ and not $p1g1$. According to the $p2mg$ selection rules Γ_4-bands can only be observed with light polarized along the $[1\bar{1}0]$ azimuth whereas in $p1g1$ these states can also be ionized with light polarized perpendicular to the surface (z-direction). The result of such a test is shown in Fig. 2.13 [2.57]. For the upper spectrum light polarized predominantly along $[1\bar{1}0]$ was used whereas in the lower spectrum the component of the electric field vector along $[1\bar{1}0]$ was zero. If the adsorbate symmetry were $p1g1$ the $1\pi_x^+$-state, which transforms according to Γ_4, should also be visible in the lower spectrum. Since this is not the case we conclude that the adsorbate symmetry is $p2mg$ and not $p1g1$.

The splitting of the 1π-levels has been discussed above and the experimental data basically corroborate the conclusions as is evident from Fig. 2.11. The

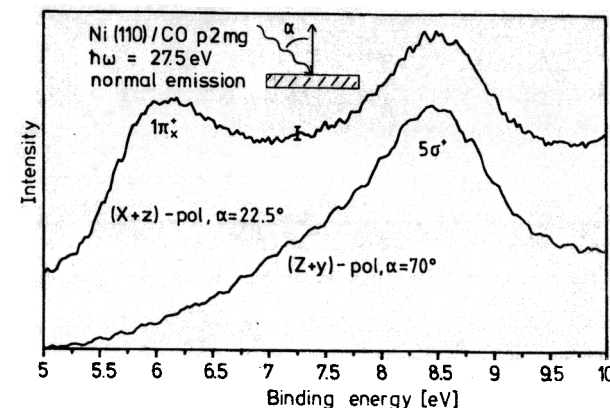Fig. 2.13. Electron distribution curves in the range of the $5\sigma/1\pi$-levels using X and Z polarized light

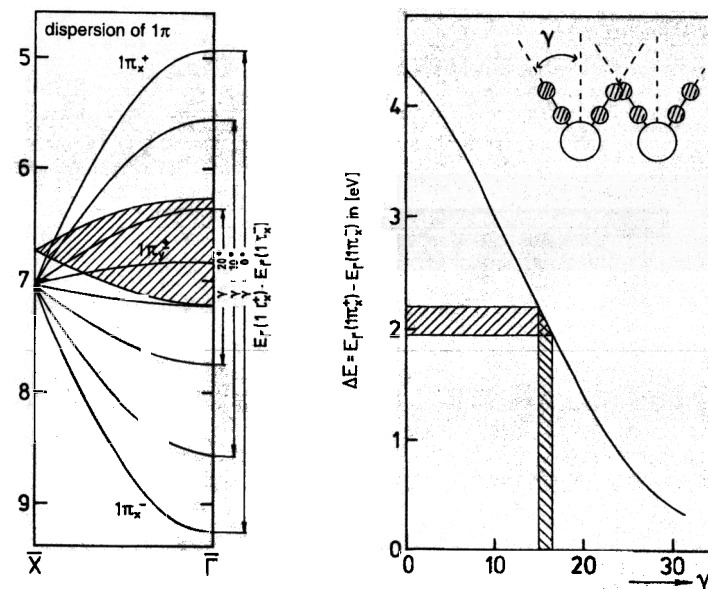Fig. 2.14. Calculated 1π-bandwidth as a function of the tilt angle of the molecular axis (γ) with respect to the surface normal. In the right hand panel the observed splitting is used to deduce the tilt angle

Table 2.1. Dipole selection rules for CO(2×1)$p2mg$

Electric field vector E	Initial state bands		
Orientation	Symmetry	Molecular assignment	Symmetry
$E\|[110]$: z-polarization	Γ_1	$4\sigma^+, 5\sigma^+, 1\pi_y^-$	Γ_1
$E\|[110]$: y-polarization	Γ_2	$4\sigma^-, 5\sigma^-, 1\pi_y^+$	Γ_2
	Γ_3	$1\pi_x^-$	Γ_3
$E\|[110]$: x-polarization	Γ_4	$1\pi_x^+$	Γ_4

strong splitting of the $1\pi_x$ components can be used -and has been used- to estimate the tilt angle of the CO molecules. The procedure can be visualized with the help of Fig. 2.14. In the left panel we show the dispersion of the $1\pi_y$- and the $1\pi_x$-bands as a function of the tilt angle γ. The $1\pi_y$-bands disperse within the

hatched area for the considered angular variations. We use the $1\pi_x$ bands as an example because for these bands the angular variations are largest so that the fitting procedure is rather precise. For $\gamma = 0°$ the splitting is calculated to be ≈ 4 eV between the bands belonging to the bonding and the antibonding combination. Note that for $\gamma = 0°$ the glide plane disappears and we reach a $p(1 \times 1)$ structure. In this case the unit cell contains only one molecule, and therefore, instead of having a splitting at Γ into two bands, the size of the Brillouin zone doubles. However, for comparison we have folded back the bands into a reduced zone, identical to the one of the $p2mg$ structure. Clearly, as soon as we allow the CO molecules to avoid each other by tilting the splitting decreases dramatically, until we reach agreement with the experimentally observed splitting of 2.2 eV at $\gamma = (17 \pm 2)°$. This is graphically shown in the panel on the right-hand side of Fig. 2.14. This strong variation of the $1\pi_x$-splitting is a consequence of the strong variation of intermolecular overlap as a function of γ. The splitting of the 1π-levels in the range of occupied orbitals should be compared with the corresponding splitting of the 2π-orbitals in the unoccupied range (Fig. 2.11). The experimental results have been taken from inverse photoemission studies of *Memmel* et al. [2.47, 48]. The observed splitting for the both the $2\pi_x$ (3.8 eV) and the $2\pi_y$ (1.2 eV) components is considerably larger than observed for the 1π-levels. This may be caused again by substrate mediated interaction due to 2π-backdonation but an additional role may be played by the 2π-wave functions themselves which are expected to be considerably more diffuse as compared with the 1π-levels. This point can be supported through a very nice series of experiments performed by *Bertel* and coworkers [2.48] on three isomorphic structures, i.e., CO $p2mg$/Ni(110), CO $p2mg$/Pd(110) and CO $p2mg$/Pt(110) where the intermolecular CO spacing varies and also the substrate mediated interaction changes. The comparison between the Ni and the Pd systems reveals that the splitting in the 2π-manifold is slightly smaller for Pd due to the increase in CO–CO separation. For Pt the situation is more complicated probably due to coupling of the unoccupied CO levels with the metal unoccupied states in this energetic range.

A direct observation of the substrate-mediated interaction is possible for the system CO $p2mg$ on Ni(110) by following the CO-induced features in the region of the metal-band structure, i.e. between the Fermi energy and a binding energy of 3 eV [2.46]. In this energy range Fig. 2.11 shows bands which exhibit dispersions of up to 0.5–1.0 eV indicating a substantial contribution via this type of interaction. Figure 2.15 shows how these features develop as a function of coverage. The states that give rise to these features are located in the surface region because they do not change their binding energy when the photon energy changes as clearly demonstrated in Fig. 2.16. At $\bar{\Gamma}$ the symmetry of the states involved can be deduced from polarization-dependent spectra (Fig. 2.17) by using Table 2.2 where the symmetry selection rules for CO-2π-derived and Ni-derived states are given under the assumption that the CO molecules are bridge-bonded [2.15–53]. The situation would change a little when the molecules were terminally bonded as suggested by *Voigtländer* et al. [2.58] because
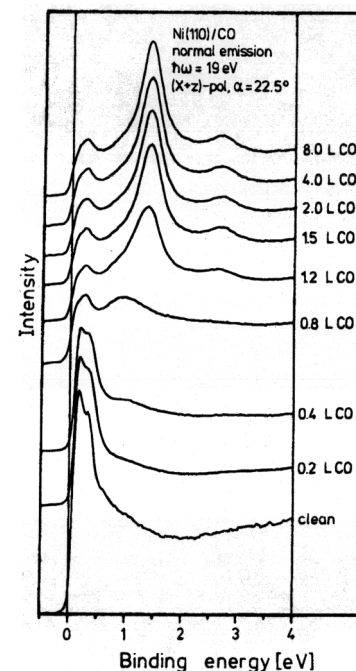

Fig. 2.15. Adsorbate induced features in the region of metal states in the system CO/Ni(110) as a function of coverage

the lateral position of the CO molecules determined the position of the mirror plane in $p2mg$ symmetry. Figure 2.18 depicts the band dispersions as determined experimentally (Fig. 2.11) superimposed onto the projected band structure of the substrate along the two azimuths, i.e. [001] and [1$\bar{1}$0] [2.59]. In the projected band structure odd and even bands are differentiated. Within the projected band structure of odd symmetry we find gaps of noticeable size and some of the observed bands change their character from surface resonances to surface states if they exist in a gap. However, a detailed analysis of the observed peak intensities and widths reveals that these properties do not change when the bands disperse into a gap. The solid lines through some of the data points are included to guide the eye and are not due to explicit calculations. The four experimental points at $\bar{\Gamma}$ in Fig. 2.18 are the π-d features shown in Fig. 2.17. The polarization dependence of these states as obtained from Fig. 2.17 can be used to identify the character of the bands of $\bar{\Gamma}$. The 2.7 eV state is excited by Z-polarized light only and thus it transforms according to Γ_1. Neglecting the $d_{x^2-y^2}$ and d_{xy}-derived bands, this feature can be identified from Table 2.2 to be the $2\pi_y^- - d_{z^2}^+ - s^+$ hybrid band. In this case the amount of s-character in the wave function cannot be ignored since the $d_{z^2} - s$ mixing is known to be strong [2.60].
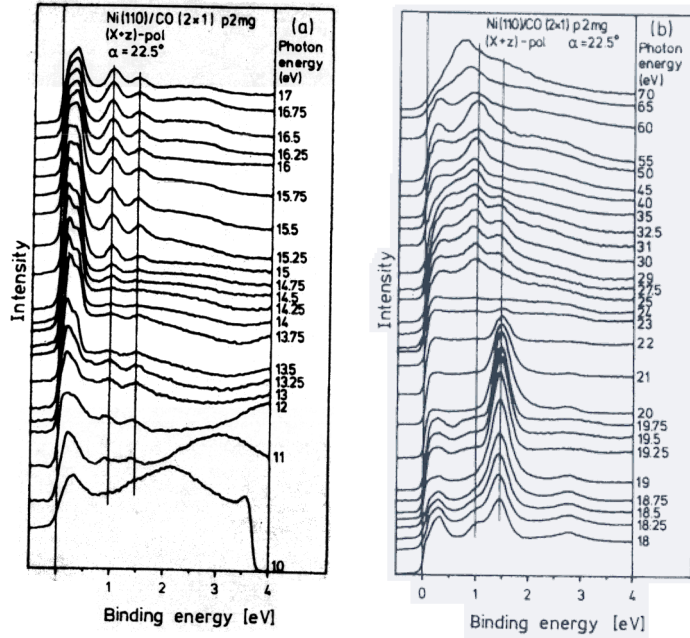
Fig. 2.16. Energy dependence of CO induced features in the region of metal states for the system CO*p2mg*/Ni(110). The spectra are taken in normal emission

Fig. 2.17. CO induced features in the range of me tal states as a functional of light polarization

In a similar fashion the 2.0 eV feature can be assigned. This state belongs to the irreducible representation Γ_2 and thus has to be one of the hybrid bands $2\pi_y^+ - d_{yz}^+$ and $2\pi_y^+ - d_{xz}^-$. To further identify this band its dispersion as shown by the solid lines in Fig. 2.18 can be considered. If this band was mainly d_{xz}^- in character at $\bar{\Gamma}$, their should not be much dispersion along $\bar{\Delta}$ because the interaction of the d_{xz}-derived bands is only weak along [001]. Figure 2.18 reveals that the dispersion bandwidth along $\bar{\Delta}$ is 0.75 eV, which is the greatest bandwidth of all observed π-d-bands. From this we assign the main character of this band to be d_{yz}^+ since the d_{yz}-orbitals interact significantly along [001], giving rise to a much greater dispersion bandwidth compared to the d_{xz}-derived bands. The remaining two π-d features at 1.0 and 1.5 eV in Fig. 2.18 are excited only by x-polarized light, indicating Γ_4 symmetry. According to Table 2.2 the metal part of their wave functions have to have d_{xz}^+- or d_{yz}^--character, respectively. An analysis like that done for the 2.0 eV-feature shows that the main character of the 1.0 eV-feature has to be d_{yz}^-, whereas the 1.5 eV-feature has to be d_{xz}^+ in character.

There are two additional bands at a binding energy of approximately 2.2 eV around $\bar{Y}$, belong to the irreducible representations Δ_1 and Δ_2, respectively. Since the Δ_1 band dispersing from 2 eV at $\bar{\Gamma}$ to 1.25 eV at $\bar{Y}$ in the first Surface

Table 2.2. Symmetry selection rules for bridge-bonded CO

Representation	CO 2π	Ni valence states	Polarization
Γ_1	$2\pi_x^-$	$s^+, d_{z^2}^-, d_{xy}^-, d_{x^2-y^2}^+$	Z
Γ_2	$2\pi_y^+$	d_{xx}^-, d_{yz}^+	Y
Γ_3	$2\pi_x^-$	$s^-, d_{z^2}^+, d_{xy}^+, d_{x^2-y^2}^-$	
Γ_4	$2\pi_x^+$	d_{xz}^+, d_{yz}^-	X
Σ_1	$2\pi_y^-, 2\pi_x^+$	$s^+, d_{z^2}^-, d_{xy}^-, d_{x^2-y^2}^+, d_{xz}^+, d_{yz}^-$	Z, X
Σ_2	$2\pi_y^+, 2\pi_x^-$	$s^-, d_{z^2}^-, d_{xy}^+, d_{x^2-y^2}^-, d_{xz}^-, d_{yz}^+$	Y
Δ_1	$2\pi_y^-, 2\pi_x^+$	$s^+, d_{z^2}^+, d_{xy}^-, d_{x^2-y^2}^-, d_{xz}^-, d_{yz}^+$	Z, Y
Δ_2	$2\pi_x^-, 2\pi_y^+$	$s^-, d_{z^2}^-, d_{xy}^+, d_{x^2-y^2}^-, d_{xz}^+, d_{yz}^-$	X

Brillouin Zone (SBZ) will, of course, also exist in the second Brillouin zone, the two experimental data points (Fig. 2.18) making up the Δ_1 band in the second SBZ around 2.2 eV may belong to this band. The Δ_2 band near $\bar{Y}$ at 2.2 eV must transform according to either Γ_3 or Γ_4 at $\bar{\Gamma}$. Table 2.2 shows that there are only two bands belonging to Γ_4 at $\bar{\Gamma}$. These are the two bands in the binding-energy range from 0.75 to 1.5 eV along $\bar{\Delta}$, and thus the Δ_2 band at 2.2 eV must belong to the representation Γ_3 at $\bar{\Gamma}$. The symmetry-selection rules in Table 2.2
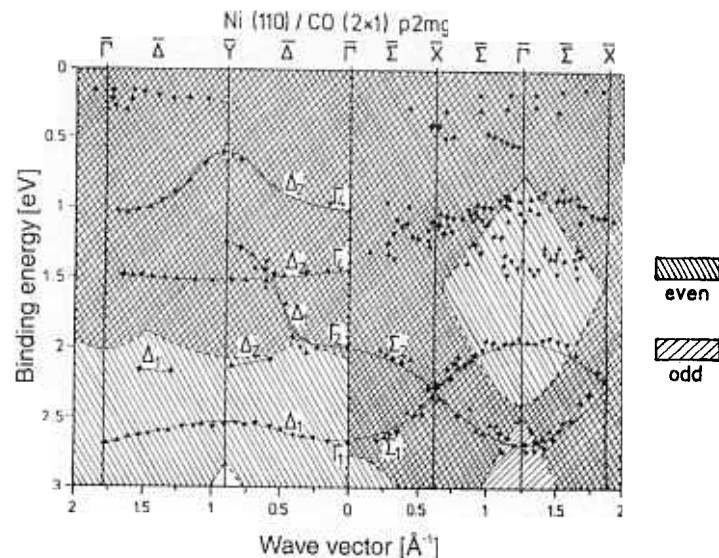
Fig. 2.18. Measured dispersions (•) of the 2π-d wavefunctions plotted on top of the calculated bull band structure projected onto the [110] surface. The projection has been done separately for even and odd bands

demonstrate that such a state cannot be exited by either polarization of the light and so this band could not be observed in the normal emission spectra.

The experimental points within 0.5 eV below E_F could not be assigned along either direction. Because the main part of the substrate emission occurs in this energetic range, these features may be due to surface umklapp processes. However, emission from hybrid bands in this energy range cannot be conclusively excluded yet [2.46].

The range from 1.0 to 1.5 eV binding energy contains many data points along $\bar\Sigma$ that could not be assigned to definite bands. In normal emission ($\bar\Gamma$) in this range only the two Γ_4 features are observed. Since the symmetry allows only twofold-degenerate bands at $\bar X$ which have to belong to different representations along $\bar\Sigma$ and at $\bar\Gamma$, the two Γ_4 bands cannot be degenerate at $\bar X$. Thus there must be two additional bands in this energetic range transforming according to either Γ_2 or Γ_3 at $\bar\Gamma$. The spectra show no additional emission in this range at $\bar\Gamma$ so that these bands will most probably belong to Γ_3 and thus will not be excitable in normal emission. In contrast to the situation near to the Fermi energy, the dispersion of the bands in the energetic range from 2 to 2.7 eV is rather clear. These bands are degenerate at $\bar X$ and their periodicity is just as demanded by the symmetry of the system. At $\bar X$ certain symmetry operations transform each of the degenerate wave functions into the other one. The band starting at 2.0 eV from $\bar\Gamma$ was assigned to have $2\pi_y^+$-d_{yz}^+-character at $\bar\Gamma$, whereas

the band starting from 2.7 eV was assigned to have $2\pi_y^-$-$d_{z^2}^+$-s^+ character. The transformation of $2\pi_y^+$ into $2\pi_y^-$ is a symmetry operation of $\bar X$, whereas the transformation of the metal part $d_{z^2}^+$-s^+ into d_{yz}^+, and vice versa, of course, cannot be done by a symmetry operation. Thus the degeneracy of these bands apparently seems not to be possible by symmetry. But, as is well known, the composition of the bands is a function of the wave vector $k_{\parallel}$ and thus the compositions of the bands at $\bar X$ will differ from their composition at $\bar\Gamma$. To discuss this in more detail, assume, for instance, that the band starting at 2.0 eV from $\bar\Gamma$ ($2\pi_y^+$-d_{yz}^+) begins to pick up $d_{z^2}^-$-s^- character when dispersing along $\bar\Sigma$. This is possible since $2\pi_y^+$, d_{yz}^+, and $d_{z^2}^-$-s^- all belong to the same irreducible representation along $\bar\Sigma$. If the second band starts to pick up d_{yz}-character, we get two bands at $\bar X$, the first one being composed of $2\pi_y^+$, d_{yz}^+, and $d_{z^2}^-$-s^-, and the second consisting of $2\pi_y^-$, d_{yz}^-, and $d_{z^2}^+$-s^+ wave functions. These bands are allowed to be degenerate at $\bar X$ if they contain corresponding metal or CO wave functions of equal amounts. This means that if, for instance, the first band contains 10% d_{yz}^+, the second one has to contain 10% d_{yz}^-. Figure 3.19 shows a plot of the wave functions of these bands at $\bar Y$, $\bar\Gamma$, and $\bar X$, assuming that the composition of the bands at $\bar Y$ does not differ from their composition at $\bar\Gamma$. It should be noted that the qualitative composition of the bands as shown in
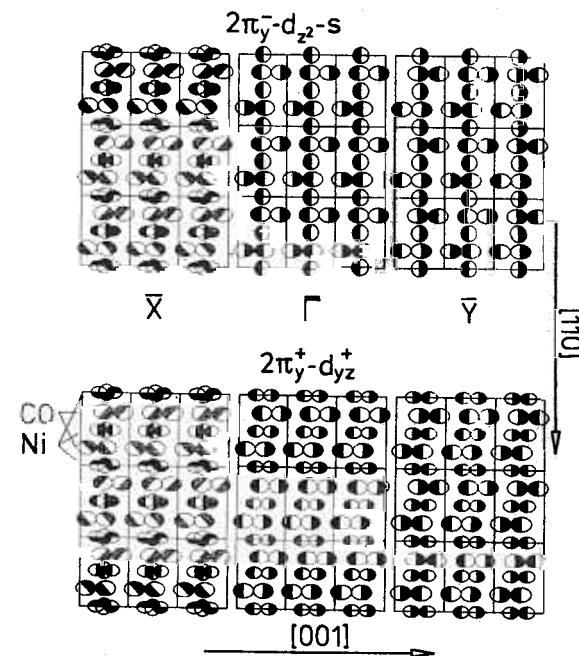

Fig. 2.19. Schematic representations of the 2π-d wave functions at different k-points. (See comments in the caption of Fig. 2.12). The positions of CO molecules and Ni atoms are marked

Fig. 2.19 at $\bar{X}$ and $\bar{Y}$ is just an arbitrary choice. There is no specific physical reason to state that this must be the right composition although it may be the correct one.

As stated above, the bands in the range from 1.0 to 1.5 eV below E_F will most probably be degenerate at $\bar{X}$ with bands belonging to Γ_3 at $\bar{\Gamma}$. For these bands the same problems must be discussed; there must also be a change in the amount of the metal character of the wave functions along $\bar{\Sigma}$.

Summarizing this section we have a full data set of the band structure of a molecular adsorbate available but a full understanding of all observed details is still not in sight although one has come some way.

b) Weakly Chemisorbed and Physisorbed Layers

The examples for dispersions in quasi two-dimensional systems were chosen so far from the many examples of strongly chemisorbed systems. One question is what happens to the dispersion when weakly chemisorbed or physisorbed systems are considered. The latter case is easy.

Figure 2.20 demonstrates how the spectra change when we gradually go from the chemisorbed CO adsorbate via the weakly chemisorbed molecule and the physisorbed molecule finally to the condensed phase [2.12, 2.61–64]. From the top of the bottom the heat of adsorption (E_{ad}) decreases from 142 kJ mol^{-1} to 19 kJ mol^{-1} [2.65–69]. This is accompanied by changes in the adsorbate spectra. In CO/Ag(111) at $T = 20$ K CO is physisorbed as documented by the small $E_{ad} = 19$ kJ mol^{-1} [2.66]. This explains why a spectrum similar to condensed CO is observed for this adsorbate. The splitting in the 5σ-emission is connected with the formation of a two-dimensional overlayer. Figure 2.21 exhibits the dispersion measured via ARUPS for the system CO/Ag(111) [2.62]. We know from a symmetry analysis that in this system the CO molecules are oriented with their axes parallel to the surface [2.63]. It is also known from LEED studies that CO and N$_2$ physisorbed on graphite form herringbone structures, as shown in the inset in fig. 2.21 [2.70]. Such structures again belong to nonsymmorphic space groups with two molecules in the unit cell. This is the reason why the molecular ionization bands appear to be split in two components, i.e., a bonding and an antibonding combination at $\bar{\Gamma}$ [2.71]. From symmetry considerations it is clear that these two bands are degenerate at the zone boundary [2.55]. The splitting is larger for the 5σ-level than for the 1π-level, which is not unreasonable on the basis of intermolecular overlap considerations. Figure 2.22 shows schematically two-dimensional wave functions of a herringbone structure based on $5\sigma, 4\sigma$-, and 1π-orbitals of CO for the center and the border of the Brillouin zone. At the Brillouin-zone center there are two split components for each orbital, a symmetric and an antisymmetric combination, i.e, two components for the 5σ- and 4σ-orbitals and four components for the 1π-orbital. Upon going from the center to the border of the Brillouin zone, the components become pairwise degenerate for similar reasons as discussed for the system CO(2 × 1) $p2mg$/Ni(110) [2.37]. The smaller splitting of the π-levels
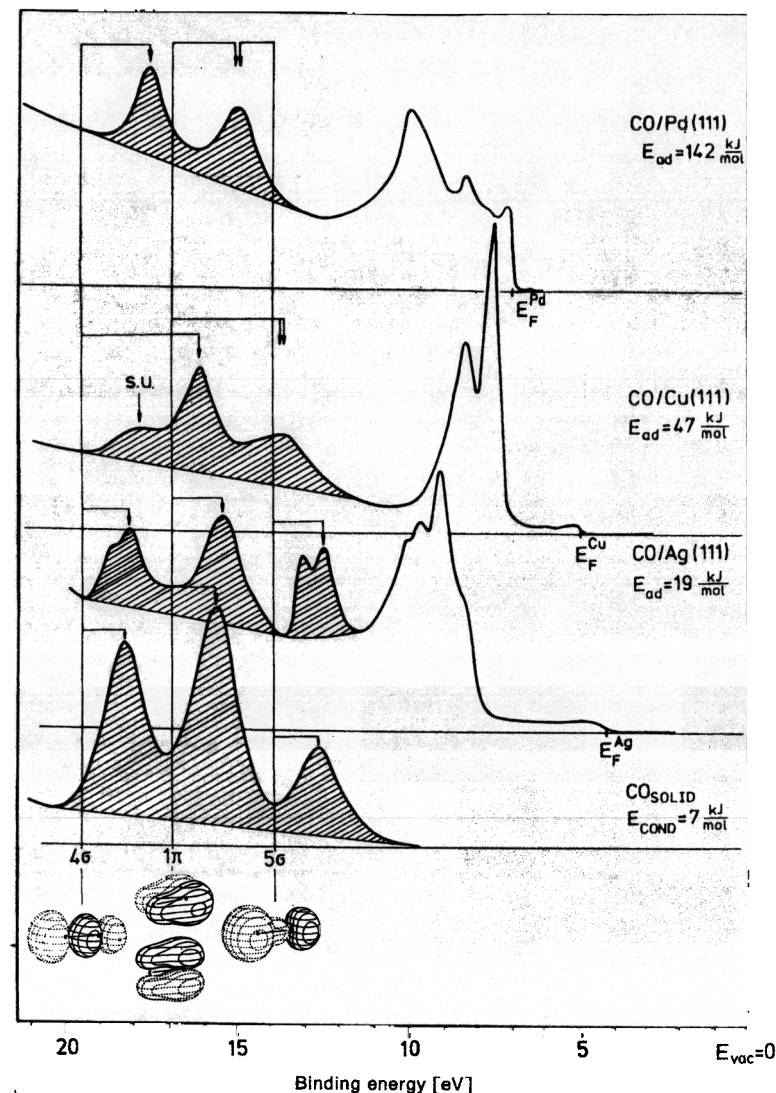

Fig. 2.20. Electron distribution curves of CO adsorbates of varying CO-substrate bond strength. For reference the gas phase values of the outer valence ionizations of CO are given

compared with the 5σ-levels can be qualitatively deduced if we estimate the overlap between neighboring molecules. Clearly, even though the radial extent of the 1π-orbitals is largest, phases are such that the total overlap cancels to a large degree. For the 5σ-orbital this is not the case as it is not for the 4σ-orbital
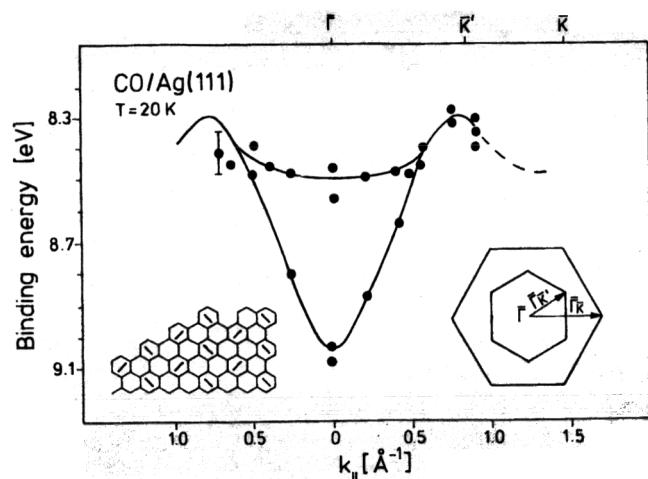
Fig. 2.21. Measured dispersions in the 5σ CO levels of CO/Ag(111)

in a herringbone structure. However, there are geometries where one could expect a strong splitting for one σ-orbital and a very small splitting for the other σ-orbital. Consider a situation where the orbitals are arranged at right angles [2.72]. Assume one orbital to be bonding, the other one to be antibonding with respect to the two nuclei as is the case for the 5σ and 4σ orbitals, respectively. If we construct two-dimensional wave functions based on both orbitals, then at the Brillouin zone center the splitting of the bands is small or even zero for the 4σ $(2\sigma_u)$ orbital, and large for the $5\sigma(3\sigma_g)$, orbital. It is quite possible that some observations in the literature [2.63] are due to such effects.

A particularly interesting observations has been made for herringbone systems if the temperature is increased. These physisorbed overlayers are known to undergo order-disorder transitions [2.70]. The CO molecules are then no longer locked into a herringbone structure but rotate freely on their site. This destroys the nonsymmorphic structure and, concomitantly, the splitting of the σ-levels disappears. CO/Ag(111) is a system where ARUPS can be used to study phase transitions in quasi-two-dimensional systems [2.62,63].

The next step in our discussion is to consider the slightly more complicated situation for the weakly chemisorbed system CO/Cu(111) [2.61] with a heat of adsorption of 47 kJ mol^{-1} [2.67]. With respect to the CO/Ag(111) system the features in the spectrum shift and the intensities of the lines are altered considerably. Three lines are still found, but their assignment is, as we shall see further below, quite different from the one for the condensed molecular solid.

The assignment of the spectrum of the CO/Cu(111) system [2.61], given in Fig. 2.20, indicates that the considerations presented so far are not complete and sufficient to explain all experimental findings. It has been shown theoretically
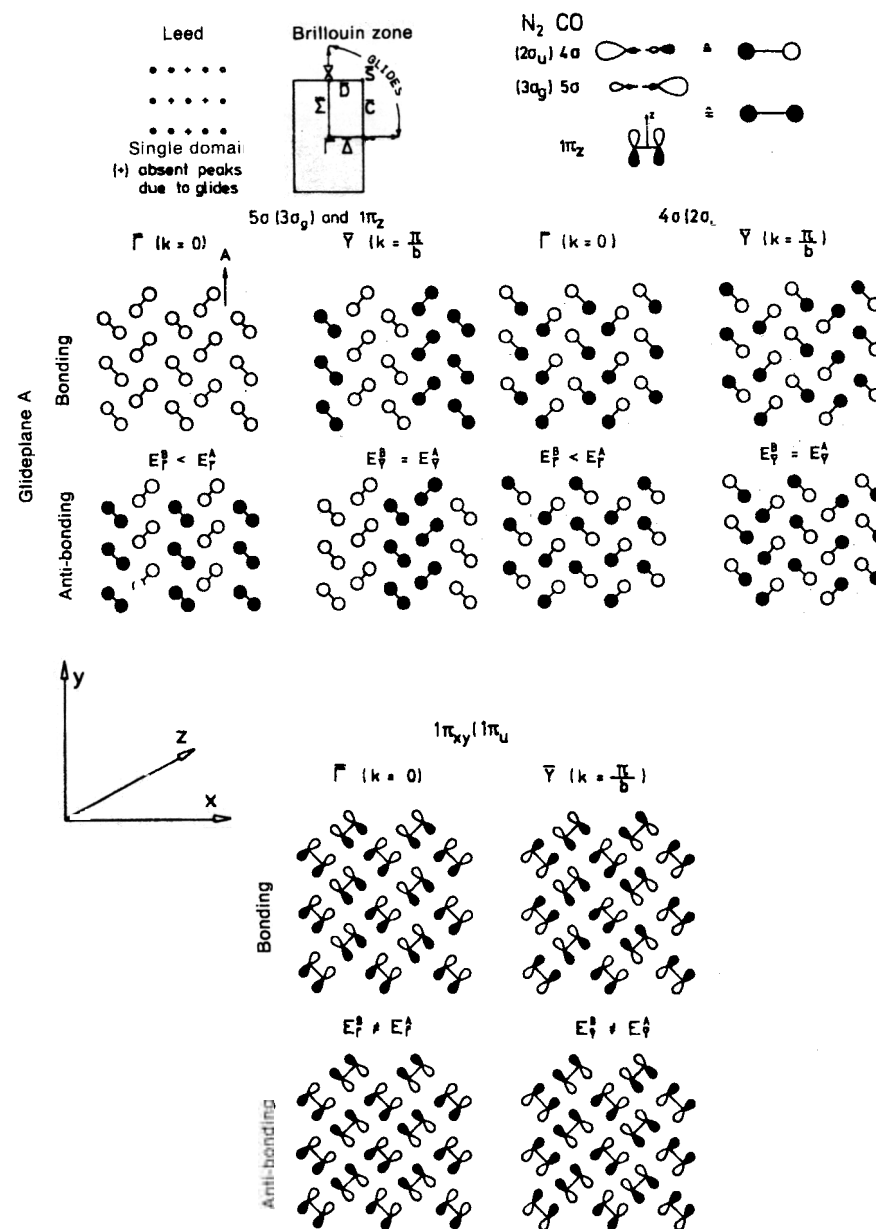
Fig. 2.22. Schematic representations of σ and π wave functions at two k-points for a herringbone structure

that for weakly chemisorbed systems so called 'shake up' excitations accompanying the 'normal' electron emission have to be considered [2.73–79]. These shake-up-excitations are manifestations of the fact that the ionization process is a rather complicated many-electron process [2.25, 80]. They can be assigned to electron excitations, in addition to electron emission. Their intensity is determined by the second matrix element in (2.2) whose magnitude is governed by the projection of the wave function of the shake-up state $^{N-1}\Psi_{e,E}$ onto the 'frozen' ion state $a_k\varphi_i$. Shake-up intensities are rather low for chemisorbed and for physisorbed systems but reach the maximum for intermediate metal-molecular coupling, i.e., weak chemisorption [2.73–80]. Again, ARUPS can be employed to support the assignment, as given in Fig. 2.20 for the CO/Cu(111) system [2.61]. If the most intense CO features were due to 1π-emission, as might be suspected by comparing the spectra of the CO/Cu(111) system with CO/Ag(111), a resonance behaviour for this particular peak would not be allowed. *Mariani* et al. [2.81] demonstrated that both bands at higher binding energy are due to states of σ-symmetry by investigating the shape resonance discussed above. The 4σ ion state as well as the accompanying shake up transition exhibited parallel resonance behaviour as expected according to the assignment in Fig. 2.20. A spectrum rather similar to the one of the CO/Cu system, but with even slightly more intense satellite structure, has been found for the system CO/Au [2.82]. In the latter system the adsorption energy is between the one for CO/Ag and CO/Cu which leads us to expect more intense satellites, and corroborates the ideas presented here.

Figure 2.23 exhibits the dispersions for the system $(\sqrt{7}\times\sqrt{7})$CO/Cu(111), for which Fig. 2.20 showed an electron distribution curve [2.35]. In this case the CO molecules are oriented perpendicular to the surface as in the case of the strongly chemisorbed systems. While the integrated $5\sigma/1\pi$-dispersion is compatible with the other CO overlayer systems, the 4σ-dispersion is considerably smaller than expected for the given intermolecular separation. The observed value is represented in Fig. 2.9 by the dashed circle. The shake-up which is – as noted above – associated with the 4σ-ionization shows almost no dispersion, but only a slight variation in relative intensity with respect to the 4σ-ionization. There are sum-rules [2.83, 84] relating intensity $A(\omega, k)$ and ionization energy (ω) of the peaks in the observed spectral function with the quasi-particle energy (ε_k^{HF}). These sum-rules are of the type

$$\varepsilon_k^{HF} = \int_{-\infty}^{+\infty} w A(w, k) dw. \tag{2.6}$$

We can apply this sum rule to the observed data and regain a dispersion indicated by the open circles in Fig. 2.23. This renormalized 4σ bandwidths can now be compared favourably with the values measured for the strongly chemisorbed systems. This shows that it is the ionization process that introduces the deviations in the observed bandwidths and not a different intermolecular interaction potential in this case.

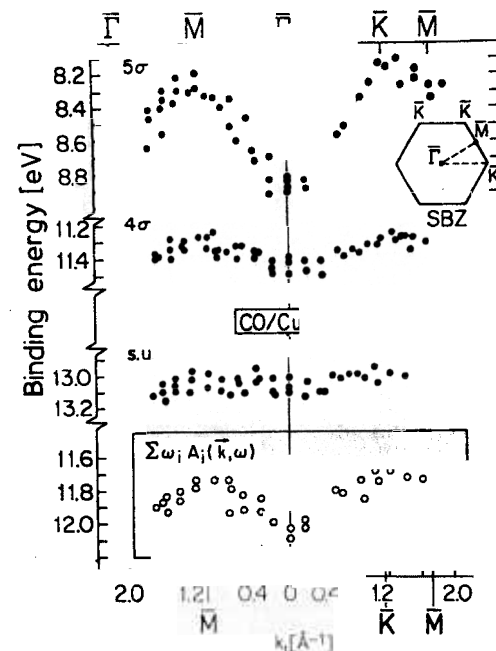With this example we finish the section on CO adsorbates and move on to chemically more complex systems.

Fig. 2.23. Measured dispersion of the CO induced levels of the system CO/Cu(111). The renormalized dispersion of the 4σ-levels is plotted as open circles

2.3 Ethylene Adsorbates [2.85]

Rather complete studies of the band structure of more complex adsorbate systems, such as chemisorbed hydrocarbons are relatively rare.

Very recently, *Steinrück* and coworkers [2.86, 87] published an interesting study of ethylene adsorption on Ni(110) where the aspect of local and global symmetry has been discussed. We want to summarize their results in the following.

Saturation coverage of Ni(110) by C_2H_4 at $T = 120$ K results in a $c(2\times4)$ LEED pattern. This pattern represents a very dense layer containing two molecules per unit cell (i.e., $\theta = 0.5$) as revealed through coverage determination with Temperature Programmed Desorption (TPD) [2.86].

The primary task, though, is, as in the case of the CO adsorbates, the determination of the local symmetry of the molecule at the surface. This is done for a dilute ethylene layer $(\theta \sim \theta_{sat}/2)$ where lateral interactions are not important. We shall see that the local geometry prevails in the dense layer. There are indications from High-Resolution Electron Energy Loss Spectroscopy (HREELS) that the ethylene species is di-σ-bonded as opposed to π-bonded with the C–C axis parallel to the surface and that the site symmetry is actually lower

than C_{2v} [2.88]. Theoretical results, however, indicate that the adsorbate bonding is quite similar in both the di-σ-bonded and the π-bonded cases, i.e., π-donation from C_2H_4 to the substrate is stronger as compared to π^*-back-donation [2.86] from the substrate towards the C_2H_4 molecule.

2.3.1 Symmetry Consideration and Ethylene-Substrate Interaction

Angle-resolved photoemission spectra of the dilute layer are shown in Fig. 2.24 [2.86]. The photon energy of 30 eV was chosen to optimize the intensity of the adsorbate-induced features. For comparison the angle-integrated photoelectron spectrum of gas-phase ethylene [2.89] including assignment is plotted. The spectra have been aligned at the $3a_g$ and $1b_{3u}$ levels (gas-phase nomenclature) as is frequently done in the literature [2.86]. The comparison reveals that the adsorbate spectrum is characteristic of a molecularly adsorbed species. It also shows that the $1b_{2u}$ ion-state is shifted by 1.1 eV to higher binding energy. This is by far the largest differential shift observed in this system. The shape of the ethylene orbitals in the gas phase is plotted in Fig. 2.25 [2.90]. It shows that the
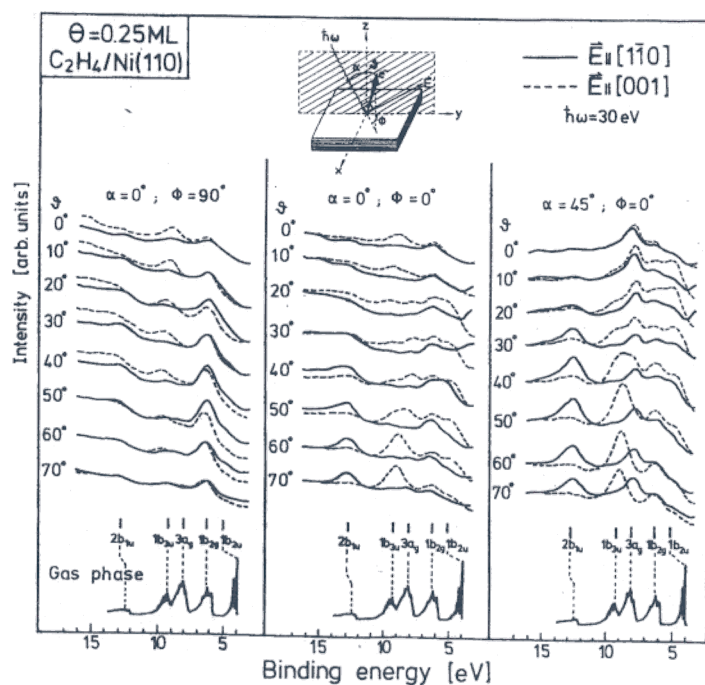

Fig. 2.24. Angle resolved electron distribution curves for a dilute C_2H_4 layer   Ni(110) in comparison to the gas phase [2.89]
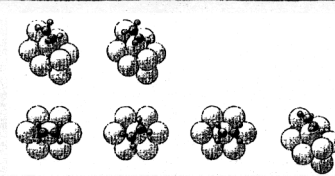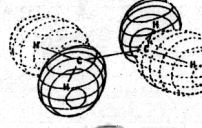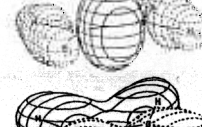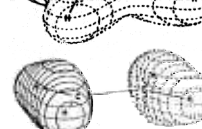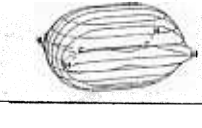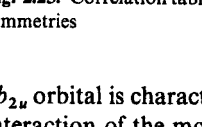

symmetry orbitals	D_{2h}	C_{2v}	C_2	$C_s(xz)$	$C_s(yz)$
	$1b_{2u}$	a_1	a	a'	a'
	$1b_{2g}$	a_2	a	a''	a''
	$3a_g$	a_1	a	a'	a'
	$1b_{3u}$	b_2	b	a''	a'
	$2b_{1u}$	b_1	b	a'	a''
	$2a_g$	a_1	a	a'	a'

Fig. 2.25. Correlation table of ethylene orbital symmetries in the gas phase with those in varying site symmetries

$1b_{2u}$ orbital is characteristic for a π-bond. The large shift indicates that the main interaction of the molecule with the surface takes place through this orbital.

The site symmetry and the orientation of the adsorbed ethylene molecules in the dilute layer can be derived from the polarization, polar angle and azimuthal dependences of the observed ionization bands, which are displayed in Fig. 2.24 and are discussed below. Figure 2.25 shows how the irreducible representations of the molecular orbitals in the isolated molecule correlate with the corresponding irreducible representations when ethylene is bound to the surface in four different point group symmetries of the hypothetical sites. The real space

geometries corresponding to the site symmetries are exhibited in Fig. 2.25. Due to the twofold symmetry of the Ni(110) surface there are two possibilities for a C_s site, as indicated.

There is an important experimental detail in the experiments by *Steinrück* and co-workers, see [2.86, 87], that must be mentioned at this point. The electron analyzer allows one to measure angular distributions of electrons by means of multichannel detection techniques including normal emission also at light incidence normal to the surface [2.91]. At these particular experimental conditions two bands ($3a_g$ at 8.0 eV and $1b_{2u}$ at 5.0 eV) show no normal emission intensity for normal incidence, but rather strong normal emission for incidence at 45°, with detection in the plane of incidence. It is clear from Fig. 2.25 that this experimental observation is strong evidence for a basically flat lying geometry. Both orbitals $3a_g$ and $1b_{2u}$ belong to the totally symmetric representation in any considered point group and are only allowed in normal emission for a non-vanishing z component of the electric field vector. Note that both orbitals show rather weak emission for normal incidence if the electrons are detected in a plane perpendicular to the incidence plane. This detection geometry is called "*forbidden*" geometry for diatomic adsorbates as discussed above. The azimuthal orientation can be extracted from the intensity variations in the $2b_{1u}$ (12.7 eV) and $1b_{3u}$ (9.2 eV) emission (Fig. 2.24). These states transform according to the b_1 and b_2 representations if C_{2v} point group symmetry is assumed. They exhibit opposite intensity variations if the plane of light incidence is changed from [001] to [1$\bar{1}$0]. The b_1 state shows strong emission in the [001] plane and weak emission in the [1$\bar{1}$0] plane, while the b_2 is weak along [001] and strong along [1$\bar{1}$0], respectively. Figure 2.25 depicts that the b_2 orbital has a node along the C–C while the b_1 orbitals has a node perpendicular to the C–C-axis. Consequently, if the electric field vector points along the C–C axis the orbital with the node perpendicular to the C–C axis (b_1) should lead to normal emission intensity, and if the electric field vector is oriented perpendicular to the C–C axis the b_2 orbital should yield electron ejection in the normal direction. From Fig. 2.24 it is therefore quite obvious that the C–C axis of the C_2H_4 molecule is to a first approximation oriented along the [1$\bar{1}$0] azimuth. However, the intensities do not completely go to zero in the appropriate directions indicating that the alignment is not perfect. In other words, the symmetry of the adsorption complex is lower than C_{2v}. This is also in line with intensity variations observed for the $1b_{2g}$ (6.2 eV) ion state which belongs to the a_2 representation in point group C_{2v}. In fact, a detailed analysis shows that the observed intensity of the a_2 ion state in normal emission can only be explained by either a slight tilting of the C—C axis, a lower symmetry adsorption site or a twisting of the molecule. *Steinrück* and the co-workers [2.86, 87] excluded the former due to the vanishing normal emission intensity of the $3a_g(a_1)$ ion state and therefore favour a lower adsorption site, i.e., slightly displaced from a high symmetry adsorption site or twisting of the molecule (Fig. 2.25).

Rösch and coworkers have analyzed the bonding via cluster calculations [2.86, 87] on the basis of the local density functional approach. Their analysis reveals that the molecule-substrate interaction follows the standard description of olefin bonding towards transition metal atoms: π-donation to the metal and backdonation from the metal ion to the π*-orbital of C_2H_4. However, the calculations do not allow discrimination between the two main adsorption modes, π or di-σ.

2.3.2 Ordered Ethylene Overlayers

After having discussed the local site geometry as determined via ARUPS on a dilute C_2H_4 layer we come back to the study of the layer at saturation coverage. *Steinrück* and co-workers [2.86, 87] demonstrated that for the strongly laterally interacting C_2H_4 layer the local site is similar to the dilute layer so that we do not have to discuss the spectra in detail in this case.

From the variation of the binding energy with the emission angle, the two-dimensional band structure of the saturated ethylene layer can be evaluated. The two-dimensional band structure has been determined along the two high-symmetry directions of the substrate, i.e. [1$\bar{1}$0] and [001]. Note that these directions are not necessarily mirror planes of the adsorbate Brillouin zone. The LEED Brillouin zone is exhibited in Fig. 2.26. The structure of the layer derived from thi: pattern is shown in the same figure. The molecules are put in the proposed asymmetric adsorption sites and are aligned along the [1$\bar{1}$0] direction with 5 Å separation. Molecules in neighbouring rows are shifted with respect to each other by 1.25 Å. This results in translational equivalence at every fourth row, i.e., a $c(2 \times 4)$ structure. The ARUPS measurements combined with molecular dynamics simulations reveal that the active intermolecular C_2H_4 potentials lead to a band structure which is not directly compatible with the Brillouin zone derived from the LEED pattern [2.86, 87]. The plot of the data as $k_{\parallel}$ vs. E_B is exhibited in Fig. 2.27. Some high symmetry points in the extended Brillouin zone scheme deduced from the LEED pattern are indicated at the top of Fig. 2.27, and it is quite obvious that the observed band dispersions do not follow the true Brillouin-zone symmetry. The observed band structure may be explained if the interaction of the molecule with the substrate is neglected for all but the π ($1b_{2u}$) ion state and the molecules are displaced with respect to each other in neighbouring rows as indicated in the middle panel of Fig. 2.28. In other words, the periodic potential leading to the fourfold repeat unit is not important. The molecular dynamics simulations energetically favour this interpretation. It is known from other hydrocarbons that the intermolecular interaction is dominated by the repulsive hydrogen-hydrogen interactions which are minimized in the geometry shown in the center panel of Fig. 2.28 with respect to the other two limiting cases (left and right panels in Fig. 2.28). Without consideration of the substrate the adsorbate unit cell only contains a single molecule. The unit cell in reciprocal space is depicted in Fig. 2.26. The experimentally chosen [001] and [1$\bar{1}$0] directions of the substrate are included in the figure. They do not represent high-symmetry directions in the adsorbate mesh, but rather the paths form $\bar{\Gamma}$ to $\bar{Y}$ along [1$\bar{1}$0]. The calculated band structure along these paths
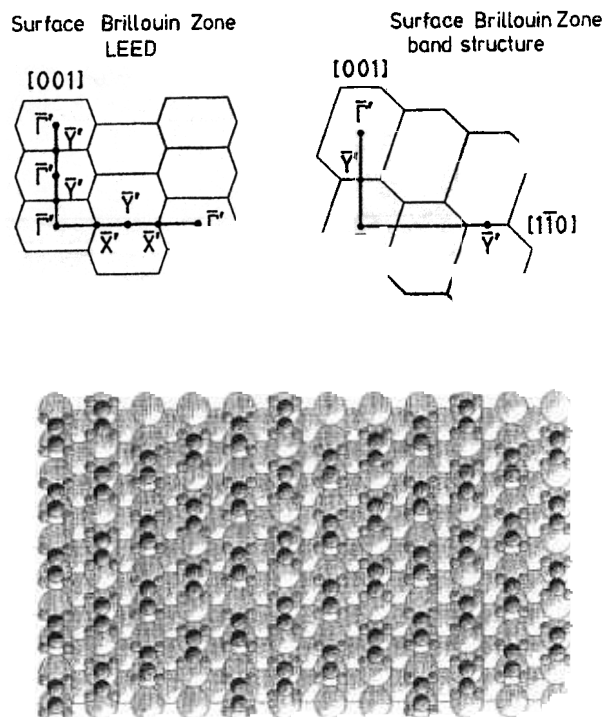
Surface Brillouin Zone
LEED
[001]

Surface Brillouin Zone
band structure
[001]

Fig. 2.26. Brillouin zones of the $c(4 \times 2)$ C_2H_4/Ni(111) system as observed with LEED (on the left) and as determined via band structure measurements (on the right). A real-space model is included

Fig. 2.27. Measured band structure for the system $c(4 \times 2)$ C_2H_4/Ni(111). Points of high symmetry according to the LEED Brillouin zone (top) and the band structure Brillouin zone (bottom) are indicated

for the energetically favoured arrangement is depicted in Fig. 2.28 (center panel) and may be directly compared with the calculated band structures for other geometries. If we now compare the calculated band structure with the measured data, as done in Fig. 2.27, we find very good agreement for four out of five ion states. The only noticable exception is the b_{2u} ion state which couples the ethylene molecule to the substrate. It is obvious that none of the other considered geometries (left and right panels) would yield a band structure that agrees with experiment anywhere near to this one. The observed dispersion can be explained on the basis of nearest-neighbour interactions. Let us consider for simplicity the [001] direction. The highest binding energy ion state has b_{1u} symmetry. The molecular wave function can be taken from Fig. 2.25. For a two-dimensional array of molecules (Fig. 2.29a) the relative phases lead to a mainly nonbonding wave function at $\bar{\Gamma}$. If for every other row of molecules the phases change at $\bar{Y}$ the nonbonding character is not changed. Consequently, there is no dispersion of this orbital along the [001] direction. The two-dimensional wave function derived from the $1b_{3u}$ orbital (Fig. 2.29b) is strongly antibonding at $\bar{\Gamma}$.
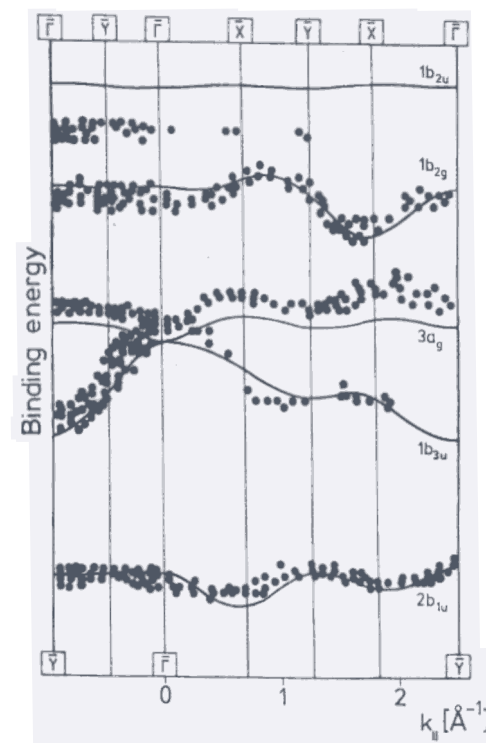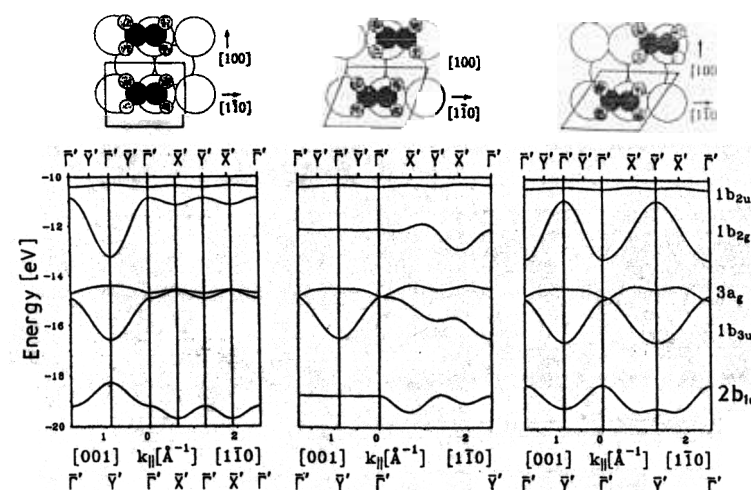

Fig. 2.28. Calculated band structures for three different lateral arrangements of C_2H_4 molecules

$\overline{\Gamma}$ $\overline{Y}$

a $2b_{1u}$

b $1b_{3u}$

c $3a_g$
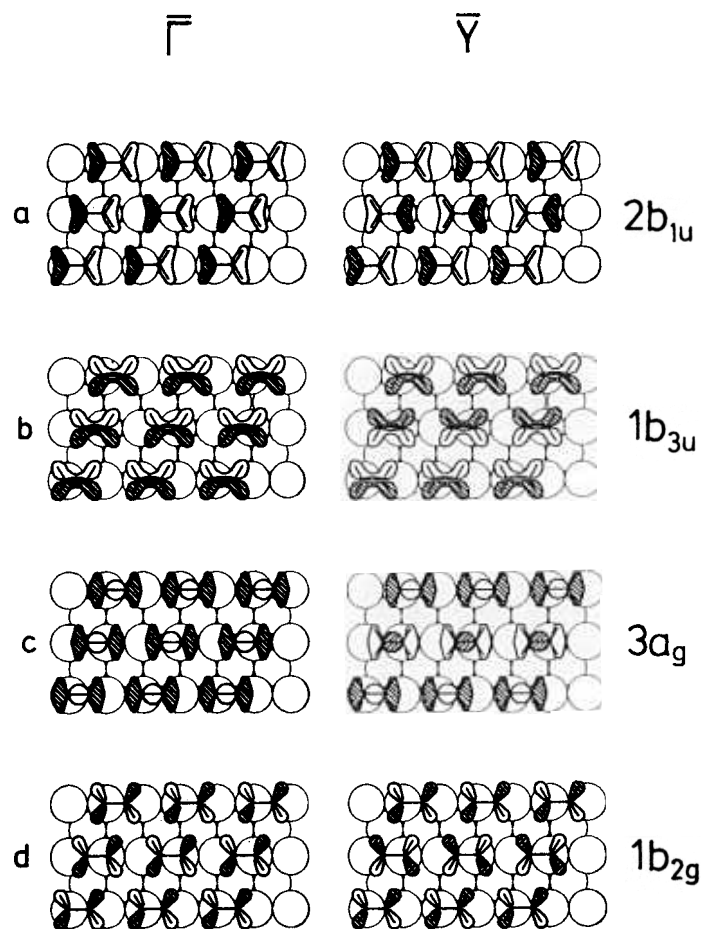
d $1b_{2g}$

Fig. 2.29a–d. Schematic two-dimensional wave functions for the ethylene overlayer for the center (left) and the border (right) of the Brillouin zone a) $2b_{1u}$, b) $1b_{3u}$, c) $3a_g$, d) $1b_{2g}$

Upon going to the zone boundary along [001] the wave function becomes strongly bonding, therefore leading to strong downward dispersion. In the case of the $3a_g$ derived wave function (Fig. 2.29c), it is essentially nonbonding or weakly bonding at $\overline{\Gamma}$. At $\overline{Y}$ it remains basically nonbonding or weakly antibonding. The $1b_{2g}$ orbital leads to a two-dimensional wave function (Fig. 2.29d). The overall character is nonbonding at $\overline{\Gamma}$ and it remains nonbonding at $\overline{Y}$. We do not expect any strong dispersion for this orbital. The b_{2u} orbital couples to the

substrate and thus we cannot expect correspondence to the simple band-structure calculation on an unsupported layer. Similar arguments hold for the other directions but they are slightly more involved because the $[1\bar{1}0]$ direction is not a high symmetry direction within the adsorbate structure.

Summarizing this section it has been demonstrated that a close packed ethylene overlayer exhibits a pronounced band structure which is completely determined by nearest neighbour interactions. The overall structure documented in the band structure is determined via ARUPS. Calculations on a free unsupported ethylene layer completely account for the observations. It should be noted that independent of the packing of the molecules, C_2H_4 occupies, almost certainly, a nonsymmetric surface site and interacts with the surface through its π-electrons. The band derived from the π-electron level does not follow the calculated band structure. It behaves like a localized state created via interaction with the substrate. The interaction with the substrate is documented predominantly in a more pronounced differential binding energy shift of this ion state.

2.4 Benzene Adsorbates

Even more complex systems which nevertheless have been extensively studied during recent years are the various benzene adsorbates. Out of the many investigations performed so far (see, e.g., Table 2.3 [2.92–113] for a selection of structures) only rather few contain detailed band structure studies.

Table 2.3. Ordered benzene overlayers on metal substrate

Substrate	Structure	θ [ML]	References
Ni(111)	$(\sqrt{7} \times \sqrt{7})R19.1°$	0.143	2.92, 113
Ni(100)	$c(4 \times 4)$	0.125	2.93
Ni(110)	$c(4 \times 2)$	0.250	2.94, 95
Ru(0001)	$(\sqrt{7} \times \sqrt{7})R19.1°$	0.143	2.96
	$(2\sqrt{3} \times 2\sqrt{3})R30°$	0.083	2.96
Rh(111)	$(2\sqrt{3} \times \sqrt{3})$rect	0.166	2.97–100
	$(\sqrt{19} \times \sqrt{19})23.4°$	0.159	2.101, 102
	$(\sqrt{7} \times \sqrt{7})R19.1°$	0.143	2.103
	$(2\sqrt{3} \times 2\sqrt{3})R30°$	0.083	2.104
Pd(110)	$c(4 \times 2)$	0.250	2.105
Pd(100)	$c(4 \times 4)$	0.125	2.106
Ag(111)	(3×3)	0.111	2.107
Os(0001)	$(\sqrt{7} \times \sqrt{7})R19.1°$	0.143	2.108
	$(\sqrt{21} \times \sqrt{21})R10.9°$	0.19	2.109
Ir(111)	(3×3)	0.111	2.110, 111
Pt(100)	$c(4 \times 4)$	0.125	2.112

We shall review in the following data gained on adsorbates on hexagonal faces and choose as an example the Ni(111) [2.92, 113] and Os(0001) [2.108] surfaces. To further discuss the determination of additional azimuthal ordering, we turn then to the analysis of a surface with twofold symmetry, i.e. Ni(110) [2.94].

a) Symmetry Considerations on Molecule-Substrate Interaction in a Dilute Disordered Layer of C_6H_6/Ni(111) [2.112]

For Ni(111) *Huber* et al. [2.113] have determined the structure for dilute layers of C_6H_6 from angle-resolved photoemission. Figure 2.30 exhibits the comparison of the angle-integrated spectrum for a disordered C_6H_6 layer at θ = 0.1 ML (θ_{sat} = 0.143 ML) with the gas-phase spectrum [2.114]. The assignment of the observed spectral features in the adsorbate to the bands of the gas-phase photoelectron spectrum has been discussed in detail by many researchers [2.92–113]. The shifts observed between gas and adsorbate phase strongly suggest that the interaction between molecules and substrate basically involves the π electrons of benzene as is well known from transition-metal benzene complexes, i.e. $(C_6H_6)_2Cr$ [2.115]. Of course, the symmetry of the molecule, which is D_{6h} in the gas phase is reduced upon interaction with the substrate at least to C_{6v}. If there is moderate interaction between molecule and substrate the threefold symmetry of the substrate is likely to reduce the sixfold molecular
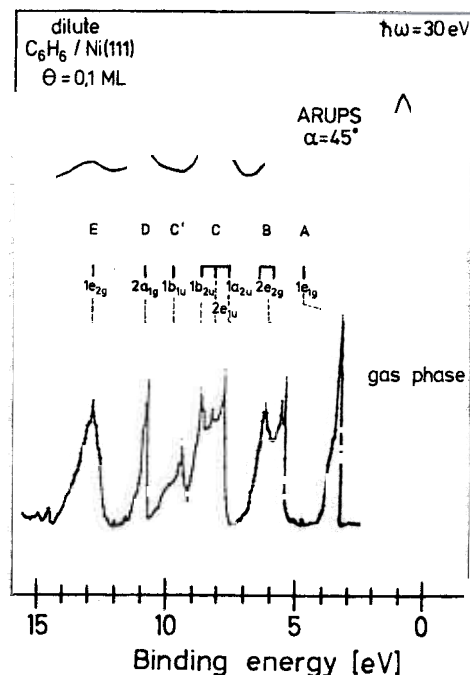
symmetry to a threefold C_{3v} symmetry. The symmetry planes may either correspond to the σ_v or the σ_d symmetry planes of the sixfold symmetry. On a surface with twofold symmetry the point group could be further reduced to C_{2v}. Figure 2.31 contains a correlation table for the molecular orbital symmetries of C_6H_6 according to the various point groups. The + and − signs correspond to allowed and forbidden normal emission of the electrons for the two limiting light polarization directions, i.e. in the ring plane (x, y) and perpendicular to the ring plane (z). Due to the broad peaks in the adsorbate spectrum some ion states are superimposed. The bands in the experimental spectrum are therefore labelled in alphabetical order. Figure 2.31 can be used to establish the symmetry of the adsorption site by evaluating the experimental data (Fig. 2.32). The spectra show negligible emission from the $2a_{1g}$ orbital for $\alpha = 0$, i.e. normal incidence and normal emission, but strong emission for $\alpha = 45°$, i.e. a non vanishing z-component of the light. Together with the fact that the b_{1u} state suggests no normal emission for both light incidence angles this proves that the ring plane is oriented parallel to the surface. From the observation that the $1b_{1u}$ state shows negligible emission at all angles whereas the $1b_{2u}$ orbital is rather

Fig. 2.30. Angle integrated photoelectron spectrum for a dilute C_6H_6/Ni(111) system in comparison with the gas phase [2.114]

Fig. 2.31. Correlation table of the orbital symmetries of C_6H_6 in the gas phase (D_{6h}) with phases in varying site symmetries. The + and − signs denote whether the orbitals can be exited with light polarized along the xy and z directions
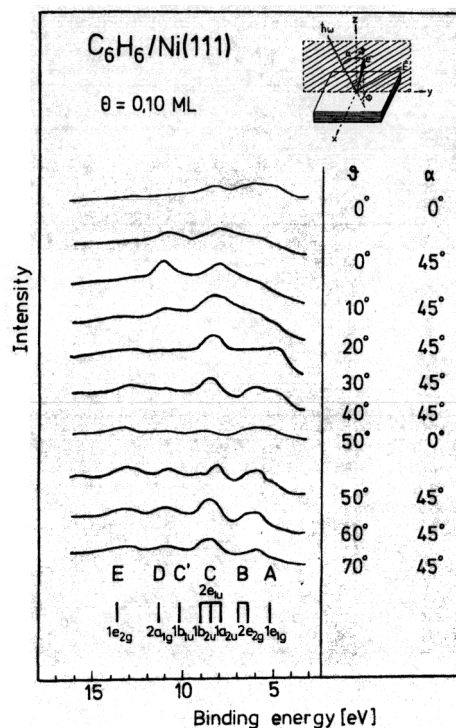
Fig. 2.32. Angle resolved electron distributions curves for a dilute C_6H_6 structures on Ni(111) surfaces a) two possible adsorption sites of isolated C_6H_6 molecules b) left panel $(\sqrt{7} \times \sqrt{7})R19.1°$ structure model; right panel $(\sqrt{21} \times \sqrt{21})R10.9°$ structure model
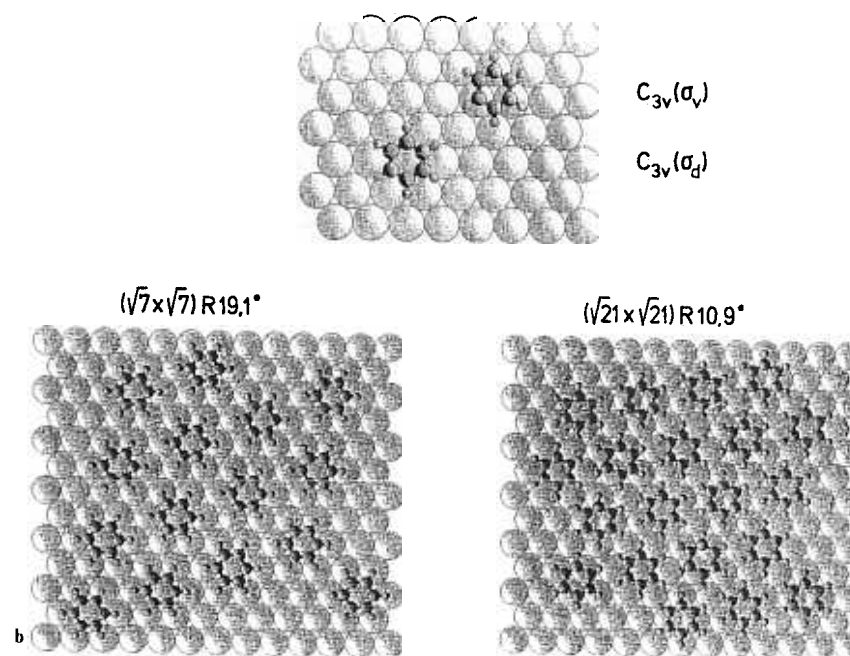

Fig. 2.33a, b. Schematic representation of the some C_6H_6 structures on (111) surfaces a) two possible adsorption sites of isolated C_6H_6 molecules b) left panel $(\sqrt{7} \times \sqrt{7})R19.1°$ structure model; right panel $(\sqrt{21} \times \sqrt{21})R10.9°$ structure model

intense we conclude that the detector is placed in the σ_d mirror plane of the molecule, indicating that this plane acts as a mirror plane for the molecular symmetry. This is then compatible with a $C_{3v}(\sigma_d)$ symmetry of the adsorbate complex. Since the spectra have been collected along the [1$\bar{1}$0] direction of the substrate *Huber* et al. [2.113] concluded that the benzene molecules are azimuthally oriented with the carbon-hydrogen bonds pointing along the [2$\bar{1}$1] directions of the substrate as shown in Fig. 2.33a. The alternative local structure with $C_{3v}(\sigma_v)$ symmetry favoured by a recent cluster calculation, shown also in Fig. 2.33a is less likely but cannot completely be ruled out because measurements were only performed in one azimuth. Thus the structure marked $C_{3v}(\sigma_d)$ depicted in Fig. 2.33a is assumed to represent the interaction of an isolated benzene molecule with a Ni(111) surface.

b) Ordered Layers: C_6H_6/Ni(111) [2.113] and C_6H_6/Os(0001) [2.108]

C_6H_6 on Ni(111) as well as on Os(0001), which are examples of close packed surfaces of a fcc and a hcp metal, form ordered overlayers of the type $(\sqrt{7} \times \sqrt{7})R19.1°$ and sometimes, i.e. on Os(0001), even more close packed layers of $(\sqrt{21} \times \sqrt{21})R10.9°$ structure. Models of these structures are shown in

Fig. 2.33b. The angle resolved spectra of a saturated $(\sqrt{7} \times \sqrt{7})R19.1°$ C_6H_6 layer on Ni(111) exhibit characteristic differences if compared with those of the dilute layer [2.113]. The spectra (not shown) indicate strong emission from the $1b_{2u}$ ion state except at particular angles. *Huber* et al. [2.113] took this as indications that the detection plane is no longer the σ_d mirror plane of adsorbed C_6H_6. An explanation would be an azimuthal rotation of the molecule due to strong lateral interactions. Figure 2.33b shows an anticipated model of the benzene layer keeping the adsorption site determined for the dilute layer, but allowing for a rotation by 30°.

Experimental evidence for strong lateral interaction is gained from the observation of dispersion of some of the ion states. Intermolecular interaction between planar hydrocarbons is mainly mediated through the hydrogen-hydrogen interaction. Therefore one expects those ion states to show the strongest effect that have large wave function coefficients at the hydrogen positions. Figure 2.31 reveals that there are several candidates. However, for a clear experimental identification of the dispersion an energetically isolated level should be used in order to avoid problems with overlapping levels. We consider the system $(\sqrt{7} \times \sqrt{7})R19.1°$ C_6H_6 on Os(0001) [2.108]. Figure 2.34 exhibits
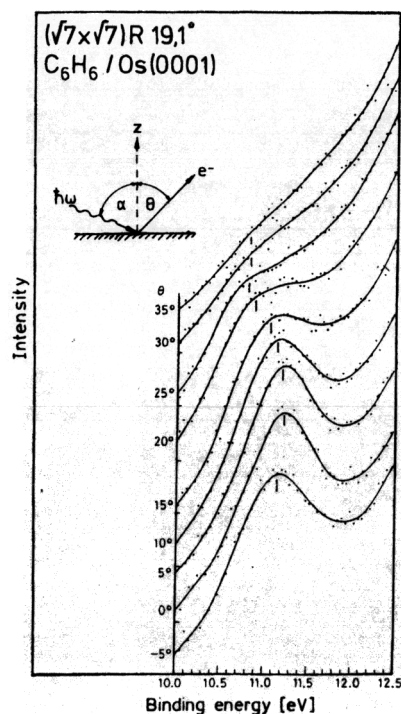
Fig. 2.34. Electron distribution curves for $(\sqrt{7} \times \sqrt{7})R19.1°$ $C_6H_6/Os(0001)$ in the range of $2a_{1g}$ ion state as a function of the emission angle θ
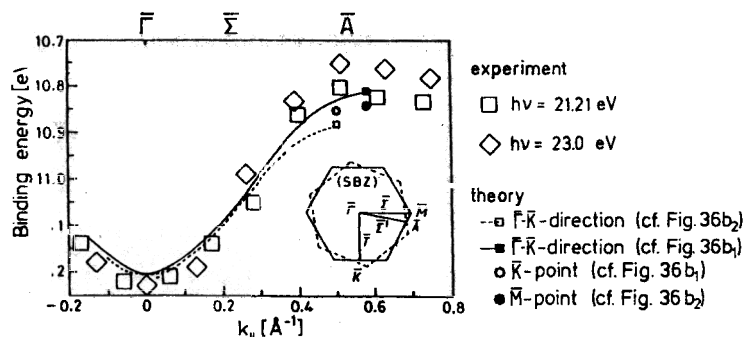

Fig. 2.35. Dispersion relation for the $2a_{1g}$ ion state of the system $(\sqrt{7} \times \sqrt{7})R19.1°$ $C_6H_6/Os(0001)$

photoelectron spectra of the $2a_{1g}$ level as a function of angle, and in Fig. 2.35 the dispersions are plotted for two photon energies along the direction indicated in the inset. The two possible domains of the overlayer are indicated. There exists a common direction $\bar{\Gamma} \to \bar{A}$ in both domains along which the experiments have

been performed. Tight-binding calculations of an unsupported benzene layer have been performed in which the relative arrangement of the molecules within the layer has been varied in order to simulate the probable structures shown in Fig. 2.36a. Two extreme cases have been chosen, i.e. a parallel arrangement (Fig. 2.36b$_1$) and an interlocked arrangement (Fig. 2.36b$_2$). Figure 2.36a obviously represents an intermediate case where the repulsion between interacting molecules is minimized. The calculated dispersion curves [2.108] are included in Fig. 2.35. They correspond to the two azimuthal directions, i.e. $\bar{\Gamma} \to \bar{K}$ and $\bar{\Gamma} \to \bar{M}$ applying intermolecular interaction parameters derived from the geometries shown in Fig. 2.36b$_1$ and b$_2$. The energy position of the band at the $\bar{M}$ point is always higher than at the $\bar{K}$ point, independent of the absolute value of the interaction parameters. The former value can be estimated almost quantitatively via a simple procedure: we consider a parallel arrangement of C_6H_6 moieties (Fig. 2.36b$_1$). On both molecules a $2a_1$-orbital is placed. The overlap between the two molecules will be dominated by the overlap of the adjacent hydrogen-atomic orbitals. The reason is that the overlap depends exponentially on the distance. A calculation of the interaction parameter β yields 0.045 eV. Since the band constructed from the $2a_{1g}$-levels is of σ-type, we expect a band dispersion from high binding energy at $\bar{\Gamma}$ to lower binding energy at the zone boundary. In the simplest version of the tight-binding theory the band dispersion of a σ-type band in $\bar{\Gamma}$-$\bar{M}$ and $\bar{\Gamma}$-$\bar{K}$ direction are given by 9β and 8β, respectively. This yields 0.4 eV and 0.36 eV if we use the above mentioned β value. Those values are very close to the dispersion plotted in Fig. 2.35 as a result of the full calculation. A similar estimate can be made for the other geometry in Fig. 2.36b$_2$. This yields 0.36 eV and 0.32 eV, respectively. In conclusion we realize that the observed dispersion can be explained on the basis of simple considerations. Very similar results have been gained for the system $(\sqrt{7} \times \sqrt{7})R19.1°$ $C_6H_6/Ni(111)$ and $(\sqrt{19} \times \sqrt{19})R23.4°$ $C_6H_6/Rh(111)$. The observed dispersions are basically the same as for the Os(0001) surface layer and have been interpreted in a similar way by *Huber* et al. [2.113] and *Neuber* [2.102].
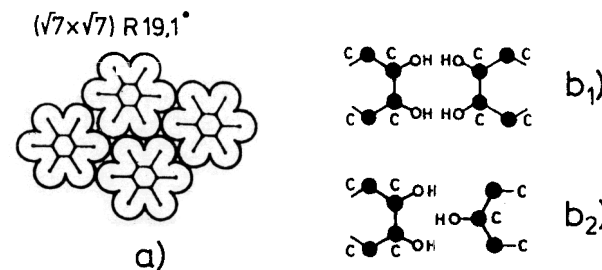

Fig. 2.36a, b. Arrangement of the C_6H_6 molecules in the $(\sqrt{7} \times \sqrt{7})R19.1°$ structure **a)** schematic representation of molecules in van der Waals contact **b)** 1: eclipsed arrangement of two C_6H_6 molecules 2: staggered arrangement of two C_6H_6 molecules

Graen and *Neumann* [2.116] have also determined the dispersion for a more densely packed layer with a $(\sqrt{21} \times \sqrt{21})R10.9°$ structure (Fig. 2.33b). Here the bandwidth increases due to the shorter nearest-neighbour distance. With such data one may now establish a bandwidth vs. distance plot quite similar to the one presented for CO adsorbates [2.102, 116].

c) Symmetry Considerations on Molecule-Substrate Interaction in a Dilute Disordered Layer of C_6H_6 of Ni[2.94]

A different situation is found for the adsorption of C_6H_6 on Ni(110). An ordered approximate $c(4 \times 2)$ structure forms for saturation coverage which shows pronounced intermolecular interactions. Before we discuss the band structure, the interaction of a C_6H_6 molecule with the surface of twofold symmetry has to be discussed. A priori, one might expect that the molecules are no longer adsorbed in a flat geometry due to the troughs of the surface, different from other close packed surfaces. In fact, such a tilt has been proposed for C_6H_6 on Pd(110) [2.117] while on the other surfaces such as Pt(110) (1 × 2) [2.118], Cu(110) [2.119] and Ag(110) [2.120, 121] flat lying geometries have been suggested. *Huber* et al. [2.94] have recently presented a very detailed study on the adsorption geometry of C_6H_6 on Ni(110). The dilute layer corresponds to a coverage of ~ 0.1 monolayer which is half of the saturation coverage. The layer is disordered. A series of angle resolved spectra is shown in Fig. 2.37. A parallel orientation of the molecule is concluded from the fact that the $2a_{1g}$ state is only observed for $\alpha = 45°$ and normal emission but at no emission angle in a plane perpendicular to the plane of light incidence. This means that the mirror planes of the benzene molecule must coincide with the [001] and [1$\bar{1}$0] directions of the substrate which is a strong indication of an azimuthally oriented benzene molecule. The $1a_{2u}$-ion state behaves similarly and corroborates the above conclusion. Obviously, the adsorbate complex seems to exhibit C_{2v} symmetry. Consequently, the doubly degenerate e-levels should split. By comparing the normal emission spectra for normal incidences obtained at the two different azimuths there are indications (e.g., at 7.8 eV and 8.1 eV) for a split $2e_{1u}$ level. A characteristic angular intensity is exhibited by the $1b_{1u}$-ion state. Its intensity is very weak for the polarization of the light along the [1$\bar{1}$0] azimuth but very strong for the light polarization parallel to [001]. Taking into account that for $\alpha = 45°$ the emission of the $1b_{1u}$ ion state is large along [001] and strongly attenuated along [1$\bar{1}$0] corroborates the orientation of the molecule with its corners along the [001] direction. The behaviour of the $1b_{2u}$ ion state is in full agreement with this conclusion. It is therefore very likely that the symmetry of the adsorbate site is C_{2v}. We should note at this point that not all levels can be simply analyzed according to the above rules. For example, the $2e_{2g}$ level shows a splitting which is due to a Jahn-Teller effect [2.122–125], also known from the free molecule. Summarizing so far we realize that the plane of the molecule is parallel to the surface and the corners are oriented along the [001] direction. The mirror planes of the molecule coincide with the [1$\bar{1}$0] and [001] directions
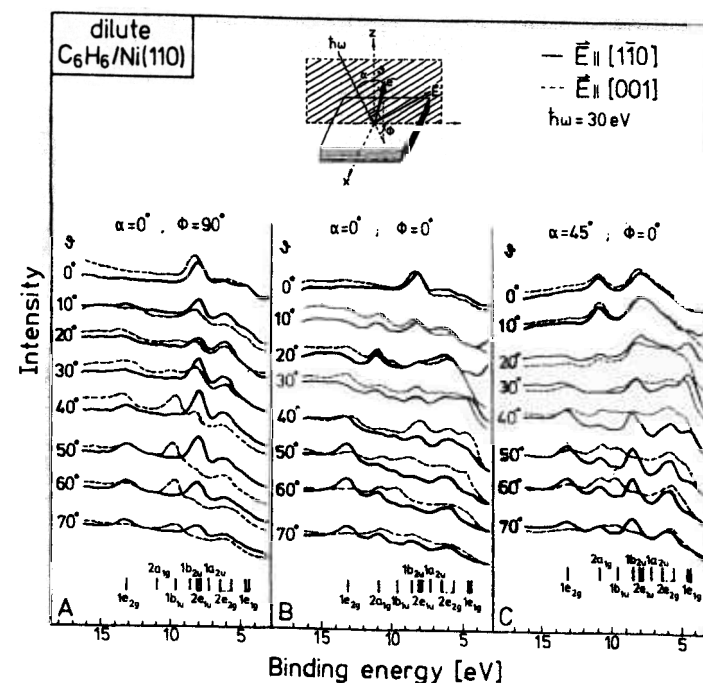
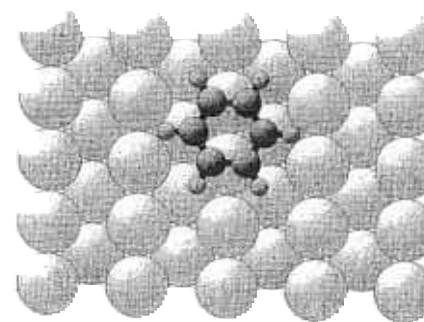Fig. 2.37. Angle resolved electron distribution curves for a dilute C_6H_6/Ni(110) system

Fig. 2.38. Schematic representation of a single C_6H_6 molecule interacting with a Ni(110) surface

of the substrate and thus the symmetry of the adsorption complex is C_{2v}. This is depicted in Fig. 2.38.

d) Ordered Overlayer: C_6H_6/Ni(110) [2.94]

The saturated layer exhibits a coverage of $\theta \sim 0.25$ ML and a $c(4 \times 2)$ LEED pattern. The angle-resolved photoelectron spectra are displayed in Fig. 2.39. The
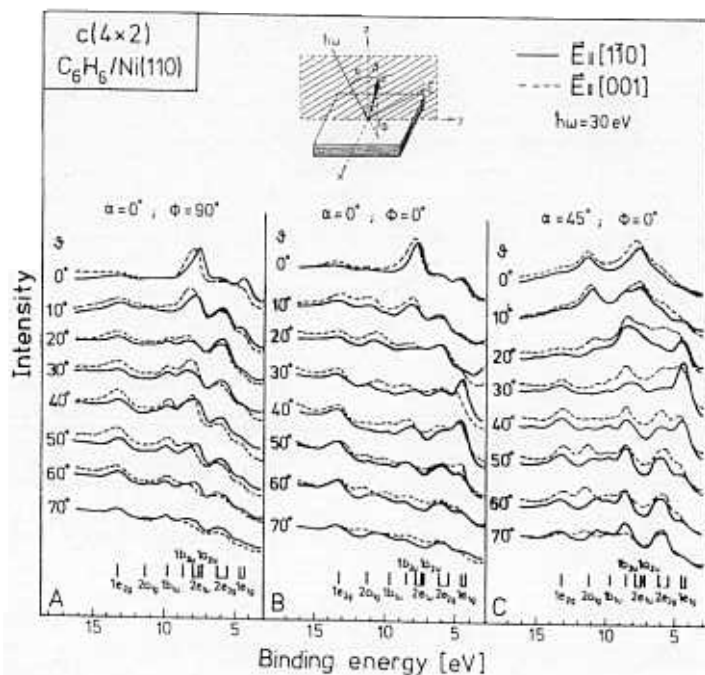
Fig. 2.39. Angle resolved electron distribution curves for a $c(4 \times 2)$ C_6H_6/Ni(110) system

parallel to the surface, azimuthally rotated with respect to the [1$\bar{1}$0] direction and at an adsorption site that is slightly asymmetric.

As mentioned above, the $2a_{1g}$ ion state exhibits significant dispersions. The band structure has been determined along the two high symmetry directions of the substrate Brillouin zone and is plotted in Fig. 2.40. Data have been obtained using various photon energies. The fact that these data coincide shows that the dispersion is caused by an electronic state with periodicity in two dimensions. The magnitude of the dispersion is 0.8 eV and thus considerably larger compared with, e.g. the $(\sqrt{7} \times \sqrt{7})R19.1°$ structure on the close packed surfaces. We shall come back to this point later. Real-space models for the approximate $c(4 \times 2)$ layer are depicted in Fig. 2.41. Figure 2.41a shows the situation if the molecules were not rotated with respect to the geometry in the dilute layer. Obviously, the van der Waals areas overlap strongly indicative of strong steric

various features in the spectra exhibit distinct polar angle and polarization dependences, but the differences are not as pronounced as for the dilute layer. Some ion states, in particular the $2a_{1g}$ orbital, show pronounced dispersions and we shall come back to this further below.

To determine the orientation of the C_6H_6 molecule in the saturated layer we resort again to the discussion of the $2a_{1g}$ and the $1a_{2u}$ ion states. From the fact that these states show significant normal emission intensity at $\alpha = 45°$, but no intensity at normal incidence, we conclude an orientation of the molecule with its molecular plane parallel to the Ni(110) surface. In contrast to the dilute layer the $2a_{1g}$ ion state of the saturated layer exhibits weak intensity in the [001] plane when the plane of light incidence is the [1$\bar{1}$0] plane. This is an indication for an azimuthal rotation of the benzene molecule with respect to the geometry in the dilute layer. Again the analysis of the $1b_{1u}$ and $1b_{2u}$ ion states provides further indications towards a structural determination. The $1b_{1u}$ as well as the $1b_{2u}$ ion state show emission intensities at all angles pointing towards an azimuthal rotation of the adsorbed molecules. A more detailed analysis of the spectra [2.94] finally leads to the conclusion that the symmetry of the adsorption complex is C_1, and that this symmetry is achieved by a molecule oriented
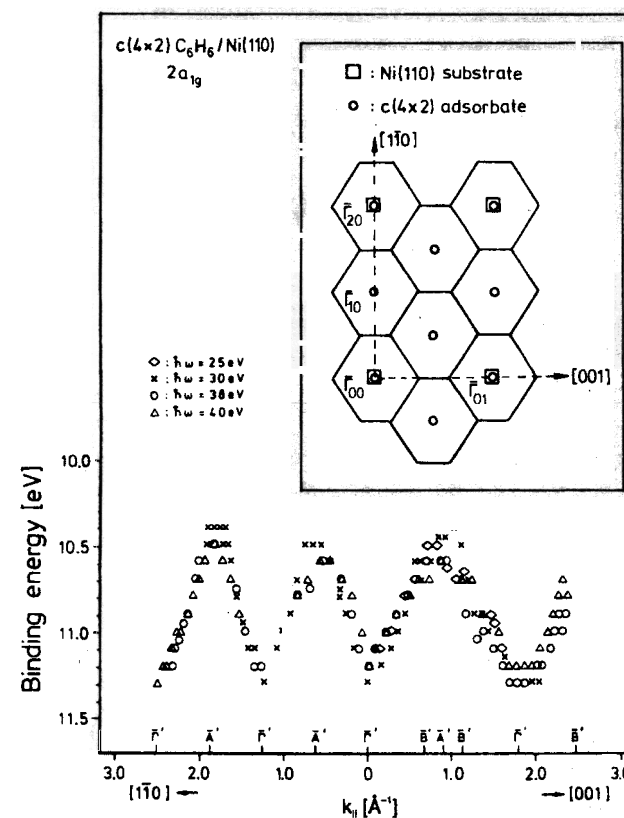

Fig. 2.40. Measured dispersion for a $c(4 \times 2)$ C_6H_6/Ni(110) system along two direction in k space as indicated in the inset
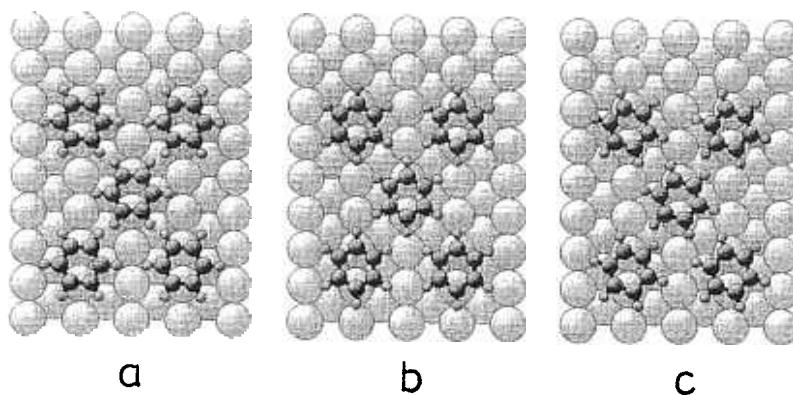
a   b   c

Fig. 2.41a–c. Schematic representations of the relative arrangements in a $c(4 \times 2)$ $C_6H_6/Ni(110)$ layer a) assuming the same site as in the dilute layer b) rotation by 30° with respect to the orientation in the dilute layer c) arrangement intermediate between a) and b)

repulsion. While the geometry in Fig. 2.41b is sterically favourable, the molecules wants to assume the local geometry as in Fig. 2.41a. The arrangement in Fig. 2.41c is therefore a compromize with reduced steric repulsion and a geometry reasonably close to the local geometry. Such an arrangement has also been favored via a force field calculation by *Fox* and *Rösch* [2.126].

As mentioned above, the dispersion in the present system is by a factor of two larger compared to C_6H_6 on Ni(110) [2.112] and Os(0001) [2.108]. This must result from the significantly closer packing of the molecules. For C_6H_6 on Ni(110) the coverage of $\theta = 0.25$ ML correspond to a unit cell area of 35.2 Å^2 with a nearest neighbour distance of 6.11 Å. This should be compared with a unit cell area of 37.6 Å^2 for the $(\sqrt{7} \times \sqrt{7})R19.1°$ structure and a coverage of $\theta = 0.143$ ML for Ni(111). The 6–7% denser packing in the layer obviously has a strong nonlinear response. This is due to the fact that the intermolecular overlaps scale exponentially with distance and, in addition, the local arrangement is such that the repulsive interaction between the hydrogen atoms is rather large. This effect has been discussed above for the $(\sqrt{7} \times \sqrt{7})R19.1°$ structure. Clearly, the interaction energy of a single C_6H_6 molecule with the metal surface must be rather strong to tolerate the considerable intermolecular repulsions in the layer which in turn leads to the pronounced band structure effects in this system.

2.5 Co-Adsorbates

Some studies [2.16, 42, 44, 45, 127] on co-adsorbate systems have been published very recently. In the following we briefly review what is known about band dispersions in ordered co-adsorbates.

The first molecular co-adsorbate systems that have been studied with ARUPS with respect to level dispersions were ordered K/CO overlayers [2.16, 42, 45, 127]. The bandwidth found for the 4σ-level of K/CO/Ru(0001) is included in Fig. 2.9 as the filled triangle. Unfortunately, the structure model for the co-adsorbate is not unique [2.124]. The CO–CO distance used in the present case is based on the assumption that a hexagonal CO overlayer is co-adsorbed with a hexagonal K overlayer, which leads to the observed (3×3) overlayer structure [2.127]. There are other structures possible, which would give shorter CO–CO distances, but the result would always lead to a relatively large bandwidth, as compared with pure CO overlayers. Obviously, the co-adsorption of K cause the 4σ wave function to change considerably, in the sense that the CO–CO interaction is mediated via the co-adsorbed potassium.

An ordered CO/O co-adsorbate on Pd(111) has been studied using ARUPS [2.42]. Figure 2.42 presents a schematic picture of the structure proposed to explain the observed (2×1) LEED pattern. Early angle-integrated photo-emission results [2.127] were basically reproduced. The co-adsorption of oxygen shifts the positions of the 4σ and $5\sigma/1\pi$ bands to higher binding energies. This has been taken as evidence for a strong oxygen CO-interaction. The 4σ dispersion is, however, basically caused by the strong lateral interaction along the CO rows. The ARUPS study shows that the 4σ dispersion, as presented in Fig. 2.9, is in line with those of pure CO adsorbates. Therefore, if there is any distortion of the wave function then it is smaller than in the case of K/CO adsorbates. Further comparison with other pure CO adsorbates on Pd(111) revealed that the observed chemical shift of the CO peaks can be explained exclusively via CO–CO interaction. Therefore, the reason for the high tendency of the CO + O/Pd(111) system to form CO_2 well below room temperature [2.128] must be due to CO–CO and O–O repulsive interactions rather than strong attractive CO–O interactions within the adsorbate.
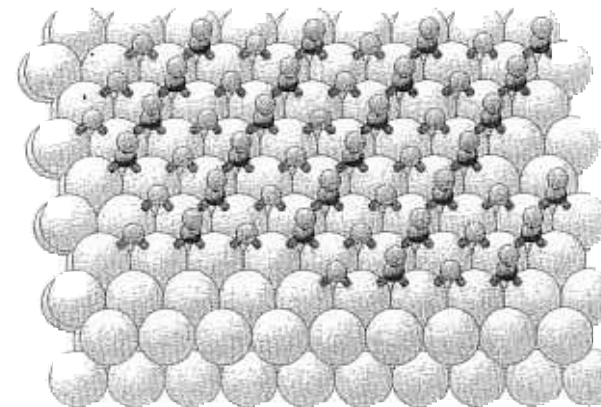

Fig. 2.42. Schematic representation of the structure of the $(2 \times 1)CO + O/Pd(111)$ co-adsorption system

2.6 Synopsis

Intermolecular interaction in adsorbates on solid surfaces can be probed via angle-resolved photoemission through the determination of band structures. Theoretical modelling allows one to extract specific parameters from the experimental observations. Some aspects are:

a) direct intermolecular interaction scales logarithmically with intermolecular distance.

b) the short-range intermolecular interaction determines the periodicity of the observed band structure.

These aspects are discussed on the basis of several examples of increasing complexity starting with CO and going via C_2H_4 to C_6H_6.

While our knowledge on pure adsorbates is growing there is very little known on co-adsorbates. We anticipate that this is a field of research of some importance in the near future.

References

2.1   I. Langmuir: J. Am. Chem. Soc. **40**, 1361 (1918)

2.2   G.A. Somorjai, M.A. Van Hove: Adsorbed monolayers on solid surfaces. *Structure and Bonding*, Vol. 38, (Springer, Berlin, Heidelberg 1979)

2.3   J.C. Tracy, P.W. Palmberg: J. Chem. Phys. **51**, 4852 (1969)

2.4   J. Koutecky: Trans. Faraday Soc. **54**, 1038 (1958)

2.5   a) T.B. Grimley: Adv. Catal. **12**, 1 (1960)
       b) T.B. Grimley: Ber. Bunsenges. Phys. Chem. **75**, 1003 (1971)

2.6   T.L. Einstein, J.R. Schrieffer: Phys. Rey. B**7**, 3629 (1973)

2.7   J.C. Tracy: J. Chem. Phys. **56**, 2736 (1972)

2.8   B.N.J. Persson: Surf. Sci. **258**, 451 (1991)

2.9   J.M. Szeftel, S. Lehwald, H. Ibach, T.S. Rahman, J.E. Black, D.L. Mills: Phys. Rev. Lett. **51**, 268 (1983)
       J.P. Toennies: Experimental determination of surface phonons by helium atoms and electronic energy loss spectroscopy, in I, *Surface Phonons*, ed. by Wikress, G.W. de Wette, Springer Ser. Surf. Sci., Vol. 21 (Springer, Berlin, Heidelberg 1991) Chap. 5

2.10   J. Fink: *"transmission electron energy loss spectroscopy"*, in *Unoccupied Electronic States*, ed. by J.C. Fuggle, J.E. Inglesfield, Topics Appl. Phys., Vol. 69 (Springer, Berlin, Heidelberg 1992), Chap. 7 and references therein

2.11   S.D. Kevan (ed.) *Angle Resolved Photoemission: Theory and Current Applications*, (Elsevier, Amsterdam 1992) and references therein

2.12   K. Horn, M. Scheffler, A.M. Bradshaw: Phys. Rev. Lett. **41**, 822 (1978)

2.13   H. Jones: *The Theory of Brillouin Zones and Electronic States in Crystals* (North-Holland, Amsterdam 1975)

2.14   H.-J. Freund, M. Neumann: Appl. Phys. A**47**, 3 (1988)

2.15   F. Greuter, D. Heskett, E.W. Plummer, H.-J. Freund: Phys. Rev. B**27**, 7117 (1983)

2.16   D. Heskett, E.W. Plummer, R.A. de Paola, W. Eberhardt, F.M. Hoffmann: Surf. Sci. **164**, 490 (1985)

2.17   N.D. Shinn: J. Vac. Sci. Technol. A**4**, 1351 (1986)
       N.D. Shinn, T.E. Madey: Phys. Rev. Lett. **53**, 2481 (1984)
       N.D. Shinn, T.E. Madey: J. Chem. Phys. **83**, 5928 (1985)

2.18   R.S. Saiki, G.S. Herman, M. Yamada, J. Osterwalder, C.S. Fadley: Phys. Rev. Lett. **63**, 283 (1989)
       D.W. Moon, S.L. Bernasek, D.J. Dwyer: Surf. Sci. **163**, 215 (1985)

2.19   F. Zaera, E. Kollin, J.L. Gland: Chem. Phys. Lett. **121**, 464 (1985)

2.20   E.W. Plummer, W. Eberhardt: Adv. Chem. Phys. **49**, 533 (1982)

2.21   G. Odörfer: CO_2-Adsorption auf Palladium (111). Diplomarbeit, Universität Erlangen-Nürnberg (1987)

2.22   C.L. Allyn, T. Gustafsson, E.W. Plummer: Chem. Phys. Lett. **47**, 127 (1977)

2.23   J. Hermanson: Solid State Commun. **22**, 9 (1977)

2.24   K. Jacobi, M. Scheffler, K. Kambe, F. Forstmann: Sol. State Commun. **22**, 17 (1977)
       M. Scheffler, K. Kambe, F. Forstmann, Solid State Commun. **25**, 93 (1978)

2.25   L.S. Cederbaum, W. Domcke: Adv. Chem. Phys. **36**, 205 (1977)

2.26   G. Borstel, M. Neumann, M. Wöhlecke: Phys. Rev. B**23**, 3121 (1981)

2.27   R.J. Smith, J. Anderson, G.J. Lapeyre: Phys. Rev. Lett. **37**, 1081 (1976)

2.28   G.J. Lapeyre, J. Anderson, R.J. Smith: Surf. Sci. **89**, 304 (1979)

2.29   G. Blyholder: J. Phys. Chem. **68**, 2772 (1964)

2.30   G. Blyholder: J. Vac. Sci. Technol. **11**, 865 (1974).

2.31   J.W. Davenport: Theory of photoemission from molecules in the gas phase and solid surfaces. PhD Thesis, University of Pennsylvania (1976), and Phys. Rev. Lett. **36**, 945 (1976)

2.32   E.W. Plummer, T. Gustafsson, W. Gudat, D.E. Eastman: Phys. Rev. A**15**, 2339 (1977)

2.33   T. Gustafsson: Surf. Sci. **94**, 593 (1980)

2.34   I.P. Batra, K. Hermann, A.M. Bradshaw, K. Horn: Phys. Rev. B**20**, 801 (1979)

2.35   H.-J. Freund, W. Eberhardt, D. Heskett, E.W. Plummer: Phys. Rev. Lett. **50**, 768 (1983)

2.36   K. Horn, A. M. Bradshaw, K. Jacobi: Surf. Sci. **72**, 719 (1978)

2.37   H. Kuhlenbeck, M. Neumann, H.-J. Freund: Surf. Sci. **173**, 194 (1986)

2.38   R. Miranda, K. Wandelt, D. Rieger, R.D. Schnell: Surf. Sci. **139**, 430 (1984)

2.39   K. Horn, A.M. Bradshaw, K. Hermann, I.P. Batra: Solid State Commun. **31**, 257 (1979)

2.40   P. Hofmann, J. Gossler, A. Zartner, M. Glanz, D. Menzel: Surf. Sci. **161**, 303 (1985)

2.41   D. Rieger, R.D. Schnell, W. Steinmann: Surf. Sci. **143**, 157 (1984)
       P. Hofmann, S.R. Bare, D.A. King: Surf. Sci. **117**, 245 (1982)

2.42   G. Odörfer, E.W. Plummer, H.-J. Freund, H. Kuhlenbeck, M. Neumann: Surf. Sci. **198**, 331 (1988)

2.43   C.W. Seabury, E.S. Jensen, T.N. Rhodin: Solid State Commun. **37**, 383 (1981)

2.44   D. Heskett: Private commun. (1986)

2.45   C. Schneider, H.-P. Steinrück, T. Pache, P.A. Hemann, D.J. Coulman, E. Umbach, D. Menzel: Vacuum **41**, 730 (1990)

2.46   H. Kuhlenbeck, H.B. Saalfeld, U. Buskotte, M. Neumann, H.-J. Freund, E.W. Plummer: Phys. Rev. B**39**, 3475 (1989)

2.47   N. Memmel, G. Rangelov, E. Bertel, V. Dose, K. Kometer, N. Rösch: Phys. Rev. Lett. **63**, 1884 (1989)

2.48   G. Rangelov, N. Memmel, E. Bertel, V. Dose: Surf. Sci. **251/252**, 965 (1991)

2.49   D.A. Wesner, F.P. Coenen, H.P. Bonzel: Phys. Rev. Lett. **60**, 1045 (1988)

2.50 W. Riedl, D. Menzel: Surf. Sci. **163**, 39 (1985)
2.51 R.J. Behm, G. Ertl, V. Penka: Surf. Sci. **160**, 387 (1985)
2.52 S. Haq, J.G. Love, D.A. King: Surf. Sci. **275**, 170 (1992)
2.53 D.J. Hannamann, M.A. Passler: Surf. Sci. **203**, 449 (1988)
2.54 N. Pangher, J. Haase: Verhandlg. Dt. Phys. Ges. 17A, SF37.6 (1993)
2.55 F. Hund: Z. Phys. **99**, (1936)
2.56 a) D.B. Litvin: Thin Solid Films **106**, 203 (1983)
      b) D.B. Litvin: J. Phys. C **17**, L37 (1984)
2.57 H. Kuhlenbeck: Charakterisiermig des elektronischen Eigenschaften des Adsorbatsystems Ni(110)/CO(2 × 1)p2mg mittels Winkelaufgelöster Photoelektronenspektroskopie. Dissertation, Universität Osnabrück (1988)
2.58 B. Voigtländer, D. Bruchmann, S. Lehwald, H. Ibach: Surf. Sci. **225**, 1521 (1990)
2.59 M. Donath: Private commun. (1992)
2.60 J. Noffke: Private commun. (1992)
2.61 H.-J. Freund, W. Eberhardt, D. Heskett, E.W. Plummer: Ann. Isr. Phys. Soc. **6**, 185 (1983)
2.62 D. Schmeisser, F. Greuter, E.W. Plummer, H.-J. Freund: Phys. Rev. Lett. **54**, 2095 (1985)
2.63 W. Hansen, M. Bertolo, K. Jacobi: Surf. Sci. **253**, 1 (1991)
2.64 W. Eberhardt, H.-J. Freund: J. Chem. Phys. **78**, 700 (1983)
2.65 R.C. Weast: *CRC Handbook of Chemistry and Physics*, 54th ed., (The Chemical Rubber Company, Cleveland 1973)
2.66 G. McElhiney, H. Papp, J. Ritchard: Surf. Sci. **54**, 617 (1976)
2.67 J. Kessler, F. Thieme: Surf. Sci. **67**, 405 (1977)
2.68 K. Christmann, O. Schober, G. Ertl: J. Chem. Phys. **60**, 4719 (1974)
2.69 H. Conrad, G. Ertl, J. Koch, E.E. Latta: Surf. Sci. **43**, 462 (1974)
2.70 R.D. Diehl, S.C. Fain: Surf. Sci. **125**, 116 (1983)
2.71 M. Seel, H.-J. Freund: Solid State Commun. **55**, 895 (1985)
2.72 M. Gumbiowski, V. Staemmler: Private commun. (1991)
2.73 K. Hermann, P.S. Bagus, C.R. Brundle, D. Menzel: Phys. Rev. **B24**, 7025 (1981)
2.74 R.P. Messmer, S.H. Lamson: Chem. Phys. Lett. **65**, 465 (1979)
2.75 H.-J. Freund, E.W. Plummer: Phys. Rev. **B23**, 4859 (1981)
2.76 K. Schönhammer, O. Gunnarsson: Solid State Commun. **26**, 399 (1978)
2.77 D. Saddei, H.-J. Freund, G. Hohlneicher: Surf. Sci. **95**, 257 (1980)
2.78 E. Umbach: Surf. Sci. **117**, 482 (1982)
2.79 N. Mårtensson, A. Nilsson: J. Electron Spectrosc. Relat. Phenom. **52**, 1 (1990)
2.80 G. Wendin: *Structure and Bonding* Vol. 45, (Springer, Berlin, Heidelberg 1981)
2.81 C. Mariani, H.-U. Middelman, U. Iwan, K. Horn: Chem. Phys. Lett. **93**, 308 (1982)
2.82 H.P. Bonzel: Private commun. (1980)
      A. Sandell: Autoionization studies of adsorbates, Thesis, Uppsala University (1993)
2.83 L. Hedin: Phys. Scr. **21**, 477 (1980)
2.84 B.I. Lundqvist: Phys. kondens. Materie **6**, 193 (1967)
      B.I. Lundqvist: Phys. kondens. Materie **7**, 117 (1968)
      B.I. Lundqvist: Phys. kondens. Materie **9**, 236 (1969)
2.85 N. Sheppart: Ann. Rev. Phys. Chem. **39**, 589 (1988) and references therein
2.86 M. Weinelt, W. Huber, P. Zebisch, H.-P. Steinrück, M. Pabst, N. Rösch: Surf. Sci. **271**, 539 (1992)
2.87 M. Weinelt, W. Huber, P. Zebisch, H.-P. Steinrück B. Reichert, U. Birkenheuer, N. Rösch: Phys. Rev. **B46**, 1675 (1992)
2.88 J.A. Stroscio, S.R. Bare, W. Ho, Surf. Sci. **148**, 499 (1984)
2.89 K. Kimura, S. Katsumata, Y. Achiba, T. Yamakaki, S. Iwata: *Handbook of HeI Photoelectron Spectra of Fundamental Organic Molecules*, (Halsted New York 1981)
2.90 W.L. Jørgensen, L. Salem: *Orbitale Organischer Moleküle*, (Verlag Chemie, Weinheim 1974)
2.91 H.A. Engelhardt, W. Bäck, D. Menzel, H. Liebl: Rev. Sci. Instr. **52**, 835 (1981)
      H.A. Engelhardt, A. Zartner, D. Menzel: Rev. Sci. Instr. **52**, 1161 (1981)
2.92 H.-P. Steinrück, W. Huber, T. Pache, D. Menzel: Surf. Sci. **218**, 293 (1989)

2.93 J.C. Bertolini, G. Dalmei-Imelik, J. Rousseau: Surf. Sci. **67**, 478 (1977)
2.94 W. Huber, M. Weinelt, P. Zebisch, H.-P. Steinrück: Surf. Sci. **253**, 72 (1991)
2.95 M.G. Ramsey, D. Steinmüller, F.P. Netzer, T. Schedel, A. Santaniello, D.R. Lloyd: Surf. Sci. **251/252**, 979 (1991)
2.96 P. Jakob, D. Menzel: Surf. Sci. **201**, 503 (1988)
2.97 E. Bertel, G. Rosina, F.P. Netzer: Surf. Sci. **172**, L515 (1986)
2.98 S. Chiang, R.J. Wilson, C.M. Mate, H. Ohtani: J. Microsc. **152**, 567 (1988)
2.99 K. Markert, K. Wandelt: Surf. Sci. **159**, 24 (1985)
2.100 a) C.M. Mate, B.E. Bent, G.A. Somorjai: J. Electron Spectrosc. Relat. Phenom. **39**, 205 (1986)
      b) C.M. Mate, C.-T. Kao, G.A. Somorjai: Surf. Sci. **206**, 145 (1988)
2.101 M. Neuber, S Witzel, C. Zubrägel, H.H. Graen, M. Neumann: Surf. Sci. **251/252**, 911 (1991)
2.102 M. Neuber: Charakterisiering des reinen und des mit Kalium Versetzten Adsorptions-Systems Benzol/Rhodium (111), Dissertation, Universität Osnabrück (1992)
2.103 B.E. Koel, J.E. Crowell, C.M. Mate, G.A. Somorjai: J. Phys. Chem. **88**, 1988 (1984)
2.104 S. Uhlenbrock: Private commun. in [2.101]
2.105 F.P. Netzer: Vacuum **41**, 49 (1990)
2.106 P. Hofmann, K. Horn, A.M. Bradshaw: Surf. Sci. **105**, L260 (1981)
2.107 R. Dudde, K.H. Frank, E.E. Koch: Surf. Sci. **225**, 267 (1990)
2.108 H.H. Graen, M. Neuber, M. Neumann, G. Odörfer, H.-J. Freund: Europhys. Lett. **12**, 173 (1990)
2.109 M. Neuber: Private commun. (1993)
2.110 J.U. Mack, E. Bertel, F.P. Netzer: Surf. Sci. **159**, 265 (1985)
2.111 B.E. Nieuwenhuys, D.I. Hagen, G. Rovida, G.A. Somorjai: Surf. Sci. **59**, 155 (1976)
2.112 N.V. Richardsson, N.R. Palmer: Surf. Sci. **114**, L1 (1982)
2.113 W. Huber, P. Zebisch, T. Bornemann, H.-P. Steinrück: Surf. Sci. **258**, 16 (1991)
2.114 D.W. Turner, C. Baker, A.D. Baker, C.R. Brundle: *Molecular Photoelectron Spectroscopy*, (Wiley, London 1970)
2.115 F.A. Cotton, G. Wilkinson: *Advanced Inorganic Chemistry*, 4th ed., (Wiley, New york 1980)
2.116 H.H. Graen: Adsorption von Benzol auf Übergangsmetall oberflächen, Dissertation, Universität Osnabrück (1991)
      H.H. Graen, M. Neumann: Private commun. (1991)
2.117 F.P. Netzer, G. Rangelov, G. Rosina, H.B. Saalfeld, M. Neumann, D.R. Lloyd: Phys. Rev. B37, 10399 (1988)
2.118 M. Surmann, S.R. Bare, P. Hofmann, D.A. King: Surf. Sci. **179**, 243 (1987)
2.119 M. Bader, J. Haase, K.-H. Frank, C. Ocal, A. Puschmann: J. Physique Coll. C8, 491 (1986)
2.120 S.R. Kelemen, T.E. Fischer: Surf. Sci. **102**, 45 (1981)
2.121 A.C. Liu, J. Stöhr, C.M. Friend, R.J. Madix: Surf. Sci. **235**, 107 (1990)
2.122 G. Herzberg: *Molecular Spectra and Molecular Structure, III. Electronic Spectra and Electronic Structure of Polyatomic Molecules*, (Van Nostrand Reinhold, New York 1966)
2.123 H. Köppel, L.S. Cederbaum, W. Domeck: J. Chem. Phys. **89**, 2023 (1988)
2.124 J. Eiding, W. Domcke, W. Huber, H.-P. Steinrück: Chem. Phys. Lett. **180**, 133 (1991)
2.125 M. Neumann, J.U. Mack, E. Bertel, F.P. Netzer: Surf. Sci. **155**, 629 (1985)
2.126 T. Fox, N. Rösch: Surf. Sci. **256**, 159 (1991)
2.127 J.J. Weimer, E. Umbach, D. Menzel: Surf. Sci. **159**, 83 (1985)
2.128 H. Conrad, G. Ertl, J. Küppers: Surf. Sci. **76**, 323 (1978)